Final Technical Report (FTR)

Federal Agency: Department of Energy

Award Number: DE-EE0008006

Project Title: Robust and resilient coordination of feeders with uncertain distributed energy resources: from real-time control to long-term planning

Principal Investigator: Mads Almassalkhi

Assistant Professor

malmassa@uvm.edu

513-404-2270 (cell)

Business Contact: Joshua Tyack

Senior Research Administrator

spa@uvm.edu

802-656-3360

Submission Date: 10/15/2020

DUNS Number: 066811191

Recipient Organization: University of Vermont (UVM)

Project Period Organization: **Start**: 09/01/2017; **End**: 08/31/2020

Submitting Official Signature: _____

Table of Contents

Acknowledgement

Executive Summary

Renewable portfolio standards and the decreasing costs of renewable energy are among many factors that are driving the proliferation of clean energy. This will lead to increasing levels of variable solar PV in electric distribution systems, which could make reliability more challenging to maintain for distribution system operators (DSOs). To facilitate reliability under high levels of solar PV, flexibility, enabled by coordinating responsive grid resources, such as smart connected appliances and PV inverters, can support the DSO in actively managing their networks. Furthermore, this flexibility also allows system operations to be optimized with respect to economic signals from wholesale energy and ancillary service markets. To enable flexible demand and ensure reliable and economical operation of distribution systems, we present a novel hierarchical scheme that actively coordinates responsive behind-the-meter grid resources, including distributed energy resources (DERs), to reliably manage each unbalanced distribution feeder and exploits the available flexibility to economically optimize the entire network. Each layer of the scheme employs advanced optimization methods at different timescales to ensure that the system operates within both grid and device limits. The hierarchy is validated in a large-scale realistic simulation based on data from the industry. Simulation results show that coordination of flexibility improves both system reliability and economics, and enables greater penetration of solar PV. Discussion is also provided on the practical viability of the required communications and controls to implement the presented scheme within a large DSO.

In this project, we bring together state-of-the-art optimization and control tools to provide a pragmatic, yet innovative hierarchical scheme for coordinating DERs at scale. The key contributions of this project include the following:

- The presented GML-FOL-STL-DER hierarchical scheme represents a novel, scalable, and practically implementable approach to the Market DSO's task of coordinating DERs while accounting for individual device and grid constraints; thereby improving reliability.

- The scheme employs optimization-based methods within each layer to ensure that DERs are utilized optimally and in a "grid-aware" manner, and then integrates the layers with feedback-based control schemes to be robust against model-mismatch and forecast errors.

- Simulation-based analysis is conducted based on realistic network models from a New York DSO which validates the coupled GML-FOL-STL operations and highlights the role and value of the proposed scheme.

Specifically, we show that the proposed scheme significantly improves voltage regulation (by 0.02pu) within a DSO that supplies 50% of demand (by annual energy) from local solar

PV while still offering market-based flexible demand services that lead to additional cost savings of 3-6%. In addition, impressive power delivery results are achieved with feeder-level tracking errors below 100kW for 2-5MW signals.

Acronyms

AC Alternating current

AGC Automatic generation control

AMI Advanced metering infrastructure

ANSI American National Standards Institute

APE Average percent error

API Application programming interface

BTM Behind-the-meter

CAISO California independent system operator

CECONY Consolidated Edison Company of New York

CPR CleanPowerResearch

DER Distributed energy resource

DSO Distribution system operator

DSSE Distribution system state estimator/estimation

DSSE-TE DSSE-topology estimator

DSSE-VE DSSE-voltage estimator

ESS Energy storage system

EVC Electric vehicle charger

EWH Electric water heater

FERC Federal Energy Regulatory Commission

FNCS Framework for Network Co-Simulation

FOL Feeder operational layer

GLD GridLab-D

GML Grid market layer

GOOSE Generic object oriented substation event

HIL Hardware-in-the-loop

HV High voltage

IAB Industry advisory board

IEC International electrotechnical commission

IL Inner loop (referring to FOL)

IoT Internet of things

ISO Independent system operator

JHU Johns Hopkins University

KKT Karush-Kuhn-Tucker

LP Linear program

LQR Linear quadratic regulator

LSTM Long-short term memory

LV Low voltage

MIP Mixed-integer program

MISOCP Mixed-integer second-order cone program

ML Machine learning

MMS Manufacturing message specification

MV Medium voltage

NERC North American electric reliability corporation

NLP Non-linear Program

NYISO New York independent system operator

OL Outer loop (referring to FOL)

DSS Distribution System Simulator (referring to Open-DSS)

OPF Optimal power flow

ORU Orange and Rockland Utility

PI Proportional integral

PM Phase margin

PMU Phasor measurement unit

PNNL Pacific Northwest National Laboratory

PV Photovoltaics

RHC Receding horizon control

RMS Root-mean-square

RMSE Root-mean-square error

SCADA Supervisory control and data acquisition

SoC State-of-charge

SOCP Second-order cone program

STL Service transformer layer

TSO Transmission system operator

US United States

UVM University of Vermont

VB Virtual battery

VP Voltage positioning

Background

In this project, we have developed and validated an advanced, scalable control framework wherein a large fleet of diverse distributed energy resources (DERs) can be managed effectively across different voltage levels within a distribution utility. The outcomes of this management is three-fold: 1) support increasing penetrations of solar PV generation; 2) ensure reliability and resilience in advanced utility grid operations; and 3) deliver valuable market services. In achieving these goals, we rely on a number of key terms and concepts that are described next.

Key project terms and concepts

- **Distributed energy resources (DERs)** represent active nodes and are made up of smart, connected plug-loads (e.g., water heaters and air conditioners) and smart solar PV inverters. These DERs are configurable in terms of appliance ON/OFF statuses and

active/reactive power PV inverter set-points[1]. The presented framework can easily be extended to consider other energy-hungry appliances, such as smart refrigerators, electric vehicle chargers (EVCs), and energy storage systems (ESSs).

- A **behind-the-meter (BTM) DER** refers to a DER that is connected on the secondary side of a service transformer (i.e., voltage level $\leq$ 480V, which is considered low-voltage or LV). Via aggregation, all BTM DERs are represented as controllable resources on the primary side of a service transformer (i.e., > 1000V, which is considered medium-voltage or MV).

- BTM, smart, connected appliances sit behind a service transformer or a set of nearby service transformers and are aggregated and abstracted into a dynamic, energy constrained representation called a **virtual batteries (VBs)**. The VB, via direct manipulation of appliance statuses, can intelligently shift loads in time (i.e., defer demand) to achieve a desired active power set-points. Since comfort/device constraints limit the duration of the shift, the VB is akin to a first-order energy storage system. For simplicity, these appliances are assumed unity-power factor and, hence, the VB represents a controllable active power resource on the primary distribution network. Any deviation above/below from baseline demand of the aggregate VB fleet represents charging/discharging behavior.

- We complement the energy-aware VB by separately aggregating **solar PV, which is represented by distributed kW-scale PV systems**, in the LV control layer. Each PV system is equipped with a smart inverter that can configure active/reactive power set-points. Since solar PV is not constrained by internal energy bounds, but rather power limits, their aggregation is separate from the VB and linear in power bounds and power generation. All aggregated PV inverters behind the same service transformer or nearby service transformers (i.e., LV control layer) are controlled via proportional pass-thru of active and reactive power set-points. The presented framework can be extended to consider smart solar PV resources on the primary network (i.e., connected at the MV-level rather than LV-level) and standard PV inverter control schemes (e.g., IEEE 1547's power factor scheme).

- We take a utility-centric approach to grid operations with DERs and, consequently, define the **distribution system operator (DSO) as the utility**, who can configure and dispatch all DERs by having pre-defined contracts in place with DER owners (e.g., a simple utility rebate for DER participation). That is, a DSO represents a wires-and-poles utility with access to the project's advanced DER coordination technology, which enhances both control and visibility. This is valuable in New York state, which is the location of the industry partner, Orange and Rockland Utility (ORU)[2]. Since the presented framework

---

[1]While NERC's official definition of a DER is limited to electricity generating assets, they have recently recommended that demand-side management of aggregated resources be included in the definition of a DER [1] since they provide similar challenges and opportunities at the T&D interface as inverter-based DERs. Since this R&D project is forward-looking in a 2030 scenario, we have taken the liberty of using the term "DER" to refer to a broader class of distributed controllable grid resources than the more narrow 2016 definition from [1].

[2]Note that Vermont's Green Mountain Power (GMP) is already deploying a utility-centric approach to

dispatches DERs with the use of live network data for more 150 feeders, it is necessary that the **utility acts as the DSO** and not a 3rd party market actor or independent DER aggregator. However, the hierarchical control architecture can be extended to include non-utility DER actors by leveraging recent work on dynamic hosting capacity [2].

- The DSO interacts with the **transmission system operator (TSO)**, which is considered a generalization of the independent system operator (ISO). The TSO's role is to define wholesale energy prices and available market services and is modeled after NYISO in New York state. While the project considers a single common set of prices and services for all feeders, it is possible to extend the framework's market layer to different set of prices and market services for different feeders.

Introduction and motivation

For a century, distribution system operators (DSOs) have managed a system wherein power flowed from large, central thermal generators in high voltage (HV) transmission networks to medium voltage (MV) primary distribution networks to low-voltage (LV) secondary distribution networks where loads consumed energy. In fact, the timescales of aggregate loads were so slow that monthly customer meter readings were sufficient for reliable grid operations. However, the last decade has seen a precipitous drop in solar PV costs [3], which together with aggressive renewable portfolio standards and public demand for clean energy has led to increasing deployments of variable and distributed generation in distribution networks. In some cases, like California, Hawaii, Vermont, and New York, high levels of solar PV generation (e.g., $> 50\%$ of energy consumed by loads) represent a fundamental engineering challenge for electric distribution system operations and will require a much more flexible electricity grid and massive efforts to electrify end use [4]. Specifically, the energy storage capability inherent to many end-use appliances is expected to underpin a flexible demand that can greatly reduce curtailment of renewable generation and support active distribution network operations [5, 6].

Thus, a future distribution feeder with the expected MWs of solar PV and flexible demand represents a grid that interacts with thousands of controllable inverters and kW-scale loads, such as thermostatically controlled loads (e.g., electric water heaters, residential air-conditioners), deferrable loads (e.g., electric vehicle chargers, smart appliances), and distributed batteries. However, the "future" is coming sooner than we think as the availability of cheap "printable" embedded hardware platforms, such as the Internet of Things (IoT), and people's desire for comfort and convenience have recently opened up a new frontier for energy digitization [7]. Indeed, as live sensing, connectivity, and computing become inexpensive, they become ubiquitous. That is, *energy technology is advancing faster than the electricity infrastructure around it.* Thus, there is a need to reconsider the role of the distribution system operators (DSOs) as solar PV (and smart inverters) is increasingly deployed and demand becomes flexible.

While it has been clear for some time that DSOs need to evolve from passive/reactive

---

DER management using advanced technology partners, such as Tesla Energy.

network managers to active network operators [8, 9, 10, 11, 12], it has been less clear how a DSO should manage the influx of 1000s of connected controllable devices (e.g., PV inverters and smart appliances) relative to changing grid and wholesale market conditions. Specifically, the coordination between a DSO's network and many DER owners and aggregators will become critically important at scale. This has spurred a multitude of advanced concepts and models for how DSOs can interact with DERs, aggregators, and whole-sale (transmission) markets [13, 14]. In this manuscript, we focus on the so-called "Market DSO" model, e.g., see [13], where the DSO performs all coordination, aggregation, and control of DERs to deliver grid services across different timescales. While such a DSO-centric model could preclude independent DER aggregators (i.e., increases regulatory complexity), the model simplifies the role of wholesale market signals from the TSO, which only interacts with the aggregated DSO resources and does not need to be cognizant of distribution network conditions or individual DER owners or aggregators. In fact, the "Market DSO" model is similar to innovative energy service provider models proposed by entities such as ConEdison of New York [15].

In market-centric DER coordination schemes, "transactive energy" can engender holistic (TSO-DSO-Aggregator) participation of DERs [16]. Some of these schemes focus on broadcasting prices directly to devices. However, with large-scale participation of DERs, transactive energy is susceptible to harmful load synchronization effects, power oscillations, and volatile prices – especially when distribution circuits constrain DER behaviors – as shown in [17]. To incorporate AC network constraints and engender "grid-aware" approaches to DER aggregation and coordination, optimization-based methods have recently gained notoriety (in big part, thanks for recent advanced in the literature on convex OPF [18, 19, 20, 21, 22]) and been been used [23] by having the aggregator's DER control be the outcome of solving an optimization problem based on AC network models and tracking a Karush-Kuhn-Tucker (KKT) point that satisfies the KKT optimality conditions. However, for non-convex AC OPF, the KKT conditions may not be sufficient to guarantee global optimality. Other optimization schemes can provide market services with VBs without exact grid models nor real-time measurements [24]. However, these methods do not directly incorporate multi-period energy constraints and the KKT point can be sensitive to exogenous disturbances.

To overcome the effect of disturbances while tracking an aggregate power signal, the literature has recently focuses on hierarchical control of DERs in microgrid settings [25]. These works generally consider using frequency and voltage droop characteristics to generate active and reactive power set-points for DERs using local measurements of frequency and voltage and compensating for the deviations, however, the local controller design often is not cognizant of network-wide conditions nor of economic signals and desired trajectories. While [26] develops a local (proportional) controller that incorporates network parameters and conditions into controller gains to minimize voltage deviations with active power injections, it does not consider system-wide power tracking objectives such as an economic trajectory that satisfies voltage limits across the feeder. Economics and network-wide controller gains are presented in [27], where a distributed averaging PI control strategy is used to ensure proportional power-sharing and economic optimality. However, since it requires extensive communication between the DERs, it may not be feasible on a larger geographic
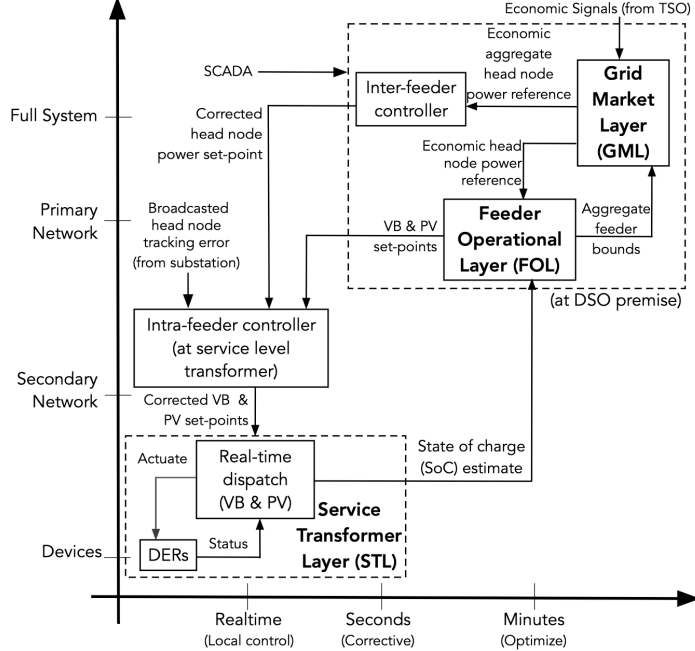
Figure 1: Hierarchical DER control scheme along qualitative spatio-temporal scales.

scale. Moreover, while the droop coefficients in [27] are chosen proportionally according to DER power limits, state-of-charge limits are not considered, and the coefficients are not optimized to minimize head node power deviations from the economic trajectory. In this paper, we overcome the above challenges associated with TSO market interactions, AC network constraints and physics, and DER control through a novel hierarchical control scheme that is practically implementable and suitable for a market DSO model.

The project's three-layer hierarchical DER coordination scheme adapts spatio-temporal concepts from conventional wide-area control (of frequency) in transmission systems to a new approach for power management in distribution systems and is summarized in Fig. 1. Recall that in conventional frequency control, primary control is performed by local droop controllers in real-time (sub-second) while secondary control balances regional areas on a timescale of 30-90 seconds and tertiary control represents economic whole-sale market clearing mechanisms for the entire system that is updated every 5-15 minutes and scheduled hourly. Together, these three layers balance supply and demand to ensure tight control of frequency. In the presented work, we decompose the DSO's operations problem as shown in Fig. 1 and summarized next:

- The **service transformer layer (STL) is tasked with performing local real-time control of a small groups of DERs** (e.g., solar PV inverters and smart appliances) every few seconds to manage power exchanges at the service transformer (i.e., the interface between primary and secondary distribution networks). This means that each STL element can be realized as a small, low-cost computing node located at the service transformer and communicating with utility's secure network and nearby DERs. Due to the local nature of control enabled by the hierarchical design, the STL controller has

8

access to the DERs' static parameters (e.g. rated power), device-level sensor measurements (e.g., temperature and PV inverter output), and device-level control inputs at each service transformer node. Each STL controller is tasked with: a) updating an aggregated dynamic flexibility model for the DERs; and b) real-time dispatch of the DERs to track certain power set-points. In particular, each STL controller constructs a dynamic representation of energy and power flexibility limits for the group of DERs at the service transformer, that together is denoted by a VB model [28, 29, 30, 31, 32]. The VB's power limits represent the (maximal) range of the control set-points that can be successfully tracked by the energy-constrained DERs at each service transformer; while VB's energy limits encode the end-user quality of service constraints and, along with the estimated state of charge (SoC), determine the duration of successful tracking performance. Different methods exist for characterizing the VB model of an aggregation of DERs, including closed-form expressions [28], optimization-based methods [29, 31], as well as deep learning techniques [30, 32]. Finally, the STL controller performs a real-time optimal control of the DERs (e.g. switching thermostatic loads on/off) to track the power set-points by explicitly accounting for service transformer and DER quality of service constraints, as necessary [31]. The active and reactive power set-points for aggregated PV inverters are provided separately to the STL and tracked via a simple proportional pass-thru operation to the individual PV inverters behind each service transformers. The STL, therefore, represents groups of diverse DERs in the secondary distribution network as dispatchable resources (i.e., VB and PV) in each phase of the primary distribution network.

- The STL's lumped resources are reflected onto the primary network, which represent a feeder's three-phase distribution network model (i.e., an unbalanced feeder). This allows the **feeder operational layer (FOL) to optimally dispatch resources in the feeder** to generate STL resource (both VB and PV) power set-points every 1-5 minutes in the entire feeder and ensure voltage and current profiles are admissible [33, 34, 35]. Thus, the FOL's objective is to coordinate the flexibility available in the STL (including responsive VBs and PV inverters) along with the (mechanically actuated) legacy control devices, such as capacitor banks (CBs) and on-load tap changers (OLTCs).

- The FOL's coordination reshapes net power exchanges at the feeders' head-nodes (i.e., at the distribution substations) in response to economically optimized power set-points provided by the **grid market layer (GML). The GML represents the DSO's scheduling coordinator** at the interface between the MV distribution system and the TSO's market and converts market signals into optimized power set-points at the distribution substation of every feeder. Since the flexibility inherent to VBs is energy-constrained and the feeders are networked within a DSO's large sub-transmission system, the GML considers a multi-period model of a simplified sub-transmission network where every feeder is represented as a PQ-load with controllable aggregated VB and PV inverter resources. In this work, the GML optimizes the DSO's resources for peak demand reduction and day-ahead and real-time balancing reserves market on a timescale of 5-15 minutes.

- Together, the three layers (GML, FOL, and STL) mirror the voltage hierarchy of the

DSO's physical HV (GML), MV (FOL), and LV (STL) network interfaces. This framework aligns with the "Market DSO" model described above and enables a scalable approach to managing millions of controllable DERs across a DSO's entire network, reliably. In addition, the presented framework also permits utilization of utility's secure and low-latency communication network between sub-transmission nodes (i.e., GML elements), distribution substation nodes (i.e., FOL elements), and service transformer nodes (i.e., STL elements). Specifically, we leverage the communication system to design and employ a proportional intra-feeder control scheme that provides sub-second updates to the FOL's power set-points to correct for forecast errors and model mismatch. Furthermore, to account for model mismatch in the GML, the DSO's SCADA system is employed to provide sub-minute inter-feeder corrective updates to the GML's economic power set-points of feeder head-nodes.

Project Objectives

The project outcome is a validated DSO technology that is commercially viable and enables cost-effective integration of solar PV generation of at least 50% of demand on an energy basis (kWh of total) by coordinating flexible distributed energy resources. The proposed technology enables a future (e.g., Year 2030) in which a large portion of BTM DERs (i.e., smart, connected appliances and PV inverters) are supporting reliability and resiliency of the grid, rather than creating reliability problems. Federal and state energy regulators are rapidly developing rules (such as FERC 2222) that will support the future of flexible demand, but those regulatory changes will take several years to become fully implemented. In the mean time, this project positions the US to lead the way in refining grid and DER technology and utility business models that will support a cost-effective and scalable transition to rapid and broad adoption of distribution-connected solar PV and accelerate US clean energy progression, while ensuring system reliability. Specifically, this project demonstrates the coming together of state-of-the-science control and optimization technologies to make the grid flexibility technically viable, cost effective at high levels of solar PV generation and reliable.

This project validates the proposed three-layer hierarchical approach shown in Fig. 1 with large-scale, realistic Transmission-Distribution-DER simulations (Task 4) based on SCADA and network data from utility partner Orange and Rockland Utility (ORU), which is as subsidiary of Consolidated Edison Company of New York (CECONY). In the simulations, more than one million active nodes (e.g., behind-the-meter DERs or flexible loads) are coordinated across ORU's subtransmission network via the GML that determines the optimal (aggregate resource) market interaction by the DSO subject to net-load forecasts (Task 3). The GML also determines the expected market contribution from each of more than 200 feeders in ORU's territory. A feeder's expected market contribution serves as the power reference signal for feeder-level aggregated resources in the FOL (Task 2). Each element in the FOL consists of one feeder and must determine the optimal dispatch of its flexible resources to satisfy the feeder-level aggregate resource reference, subject to three-phase grid

constraints (e.g., ANSI limits), mixed mechanical/discrete and electrical/continuous flexible elements, and net-load forecasts. That is, each FOL element computes power set points for the dispatchable lumped elements in the STL (Task 1).The STL's lumped resources are made up of dispatchable DERs (e.g., 50-300 diverse and heterogeneous loads and inverters), which are modeled as a VB placed in parallel with an aggregated PV inverter and is subject to stochastic bounds on active/reactive power and energy capability. These uncertain bounds (and associated distributions) are provided to the FOL to improve feeder operations under realistic variable and uncertain solar PV forecasts.

Altogether, the proposed (GML-FOL-STL) hierarchical scheme represents a scalable framework wherein in millions of resources can be coordinated within existing and/or reasonable communication requirements. However, relying strictly on market signals for operations puts reliability and resilience at risk, since we should not wait for system-wide market conditions in the GML to inform us about conditions of the grid. Therefore, we augment the above scheme to enhance responsiveness of resources by having STL and FOL elements respond to actual grid conditions akin to real-time droop control between STL elements (e.g., within a feeder) and AGC between FOL elements (e.g., between multiple feeders) to coordinate resources. This improves reliability and resilience when slower (conventional) top-down predictions do not align with actual grid conditions (e.g., a cloud drastically reduces solar PV in part of a feeder or system or DER flexibility is no longer available). For example, if one STL element cannot track its optimal set point, other STL elements, within the corresponding FOL element, must make up the difference (e.g., "pick up the slack"). If they cannot make up the difference, the FOL element is unable to track its feeder-level aggregate resource signal, so other FOL elements must make up the difference across the system. As STL or FOL elements deviate from their optimal economic reference signals, they inform upstream elements (STL-FOL-GML) of the deviation, identify their remaining available resources, and request updated reference signals using feedback control. Fig. 1 represents these controllers as the inter-feeder and intra-feeder blocks, which operate on timescales of 5-seconds and 500ms, respectively, and can operate within existing and/or state of the art smart-grid communication standards.

To achieve the project's objective, the team was led by University of Vermont (UVM) Assistant Professor and **principal investigator Mads R. Almassalkhi**, who was supported by a world-class team of scientists, academicians, students, and industry leaders.

- **University of Vermont**: Co-PIs Hamid Ossareh (Assistant Professor) and Pavan Racherla (Research Assistant Professor) were supported by Ph.D. students Nawaf Nazir and Sarnaduti Brahma and received input from Co-Is Paul Hines and Luis Duffaut Espinosa.

- **Johns Hopkins University (JHU):** Co-PIs Dennice Gayme (Associate Professor) and Enrique Mallada (Assistant Professor) were supported by Pengcheng Yang (Post-doc) and Ph.D. students Chengda Ji and Yue Shen.

- **Pacific Northwest National Laboratory (PNNL):** Co-PI Soumya Kundu was supported by research scientists Thiagarajan Ramachandran, Sai P. Nandanoori, Ankit Singhal, and Indrasis Chakraborty (now at LLNL).

- **Industrial Advisory Board (IAB)** was made up of federal and industry partners, including Dr. Dhananjay Anand from the National Institute of Standards and Technology (NIST), Mike McGuire and Aaron Anaya from ORU, Joe White from CECONY, Mark Grammatico from Clean Power Research (CPR), and Dr. Ben Hobbs who serves as CAISO Advisor.

The task structure for the project was organized as follows:
Task 1: *Aggregation, Modeling, and Real-time Coordination of DERs in the STL*
Lead: PNNL - Support: UVM.

- Groups of 50-150 diverse heterogeneous BTM DERs were aggregated and their flexibility was characterized accurately by low-order VB models. Various methods were used to develop the VB models, including (deterministic) optimization-based methods and stochastic data-driven, learning-based methods. It was shown that the VB parameters could be adapted as groups of devices were added. Different real-time coordination schemes were pursued by the team, including device-driven methods based on each device transmitting a "fitness" rating and more direct scheduling control methods. Due to the high performance of most optimization solvers today, the direct control method was shown to be sufficiently fast and was used to schedule DERs to match the aggregate with a desired set-point while managing device-specific constraints (i.e., comfort). This means that the STL is able to perform the real-time coordination of DERs to track power reference signals within 10% RMSE and characterize the bounds of flexibility with VB parameters within 10% RMSE so that the FOL can optimize the dispatch of the VBs.

Task 2: *Grid-aware Optimization and Coordination of Network Resources in the FOL*
Lead: UVM - Support: PNNL.

- Two novel unbalanced distribution OPF formulations have been developed for the FOL and interfaced with each other to schedule both mechanical/discrete legacy assets on an slow timescale, e.g., outer layer for hourly schedules for capacitor banks and LTCs, and continuously controlled assets every minute (i.e., the inner layer). The objective of the outer layer is to look ahead three hours and optimize the schedule of mechanical assets to maximize voltage margins in a simplified unbalanced model of the feeder (LinDist3) given expected feeder dispatch from the GML with as little PV inverter control/curtailment. This fixes the legacy assets' schedules and allows for the inner loop, which is a combination of a multi-period second-order conic program (SOCP) and decoupled, single-period nonlinear programs (NLPs) that together optimize the dispatch of VBs and PV inverters in the a feeder given very short-term, intra-hour PV forecasts to ensure tight tracking of head node power reference signal from the GML. The inner loop also considering power and energy constraints of the VBs and reactive power and curtailment capability of the PV inverters. The team also showed how advanced distributed system state estimation (DSSE) schemes could integrate with the FOL to provide estimated line currents (and, thus, line losses) which are used by the inner layer to ensure a zero duality gap (i.e., optimal solutions are realized and within ANSI limits). Finally, robust formulations are proposed to account for solar PV forecast uncertainties over the prediction horizon and

novel network reduction techniques were used to create accurate, significantly reduced, yet physically meaningful networks over which the FOL could optimize quickly and bring back optimized set-points of "super-VBs" to individual VBs. Overall, the FOL can solve the inner layer within a minute to provide updated VB and PV inverter set-points that are within 5% of the global optimal solution in all investigated runs.

Task 3: *Economic Dispatch and Regulation of Feeders in the GML*
Lead: JHU - Support: UVM.

- The GML dispatches available flexibility among feeders with respect to three different market signals: wholesale energy LMPs and ancillary service prices, updated every 5 minutes from NYISO, as well as peak demand charge (monthly transmission charge). Energy transactions are co-optimized with ancillary services operating reserves, and peak demand reduction. This was formulated for both radial and meshed (sub-transmission) networks of distribution substations. It was found that radial assumptions were less useful in NY's setting and a linearized OPF formulation was used with the meshed sub-transmission network extracted from NYISO's model. The GML solves the full meshed model within a couple minutes to deliver set-point updates for over 200 feeder head-nodes every five minutes. A stochastic implementation was also investigated along with financial benefit analysis which estimates the value of flexible demand in the proposed market structure for ORU as a Market DSO (i.e., the sole DER scheduling coordinator).

Task 4: *Validation and Demonstration of coupled coordination of layers*
Lead: PNNL/UVM - Support: JHU and NIST and ORU.

- Year 1 focused on proof of concept simulations of each layer separately on synthetic networks. This was advanced in Year 2 with coupled simulations under deterministic (perfect forecast) condition on small, realistic networks from utility partner and separate validation of real-time feedback-based corrective control of feeder (inter) and VB (intra) set-points with inter- and intra-feeder controllers, respectively. Year 3 included a demonstration of a browser-based visualization and analytics tool iPGA that was developed at UVM and interactively showed the effect of the FOL's dispatched flexibility and/or historical data on actual feeders. The project concluded with large-scale, stochastic simulations of all three layers on utility-provided feeders (and their reduced network approximations, which were prepared by iPGA) and NYISO-derived meshed sub-transmission network for ORU with GridLab-D. In the final large simulation, we were able to quantify the avoided voltage violations, reduced PV curtailment, and the ability to track market-signals accurately. Finally, the software tool iPGA, that was supported by this project, has been disclosed as a software invention and been licensed to startup company *Packetized Energy*, where it has been developed further into a commercial product called *GridSolver* that is now in use at utilities in the US.

Key project technical targets are shown in Fig. 2 with deliverables and milestones for the project identified as follows:

Performance Metric	FOA Metric	Proposed Target	Achieved Target
Solution components	Subset of layers	Device & Enhanced layers	Device & Enhanced layers
HiL Validation	$> 10^2$ physical nodes	$> 10^2$ with OPAL-RT	$> 10^2$ with real-time, cyber-enabled DERs
Software Validation	$> 10^6$ virtual nodes	$> 10^6$ with GridLab-D	$> 10^6$ with GridLab-D
Scalability (Feeders)	1000	>1000	>150
Scalability (Active nodes)	1,000,000	>1,000,000	>1,000,000
Computation cycle (Real-time)	1 minute	< 1 minute	< 1 minute
Computation cycle (Planning)	5 minutes	< 5 minutes	< 5 minutes
Device Time resolution (Real-time)	1 second	1 seconds	1 seconds
Device Time resolution (Planning)	1 minutes	1 minutes	1 minutes
Response time (local: STL)	< 10 seconds	Real-time	Real-time
Response time (network: FOL)	< 30 seconds	< 30 seconds	< 30 seconds
Response time (system: GML)	< 1 minute	< 1 minutes	< 1 minutes
DSSE Observability	>99%	100%	100%
Power Flows	Multiple substations	Multiple substations	Multiple substations
OPF Objectives	Techno-economic	Techno-economic	Techno-economic
Predictive Control	Real-time planning	Real-time planning	Real-time planning
Prescriptive Control	Operational planning	Operational planning	Operational planning

Figure 2: Key project metrics that have all been satisfied as proposed, except for those in orange above: *i*) the 1000 feeder setup, which has been replaced by ORU's more than 150 feeders (as ORU does not have 1000 feeders); and *ii*) we did not incorporate 100 devices for hardware testing. Instead, we showcases the viability of the proposed STL algorithms by employing > 100 real-time simulated and cyber-enabled DERs to test the viability of the presented hierarchical framework along with available IEC communication standards.

Final Deliverable #1: Completed software simulations of the GML-FOL-STL-DER hierarhcy at scale with GridLab-D.

Final Deliverable #2: Completed real-time simulations of cyber-enabled DERs.

Final Deliverable #3: Completed techno-economic benefit analysis of the project's core DSO technology

Final Deliverable #4: Work from Task 1 (STL) has been published in at least 3 peer reviewed journals and/or conferences

Final Deliverable #5: Work from Task 2 (FOL) has been published in at least 3 peer reviewed journals and/or conferences

Final Deliverable #6: Work from Task 3 (GML) has been published in at least 3 peer reviewed journals and/or conferences

Final Deliverable #7: Work from Task 4 (demonstration/validation) has been published in at least 1 peer reviewed journals and/or conferences that presents the open-source software tool iPGA suitable for demonstrating DER/solar PV "what-if scenarios" for utilities .

Final Deliverable #8: The software tool iPGA has been made available on GitHub at: https://github.com/teslauvm/ENERGISE

All major project deliverables were successfully completed.

Project Results and Discussion

Task 1: Service Transformer Layer (STL)

For Task 1, the focus in year 1 was on modeling an aggregate population of 100 or so smart appliances, which was accomplished with the VB framework in Task 1.1. In Year 2, the focus is on real-time controller performance in terms of tracking the VB's reference values with STL's available smart appliances (Task 1.2). The final year of the project was focused on integrating STL with other layers, including smart PV inverters and solar PV generation.

Task 1.1 - Modeling Aggregate Stochastic Flexibility of DERs at the STL

The goal in Task 1.1 was to build a lumped dynamic VB model of smart appliances that can suitably (within reasonable error bounds that are acceptable for robust optimization problem at the FOL) capture the short-term load response for droop-like stabilization of intra-feeder disturbances. Together with configurable smart, solar PV inverter active and reactive power injection set-points, this VB model permits STL elements within a large feeder to overcome unexpected very short-term disturbances (on the order of seconds). We then test, via simulations, the accuracy of the reduced-order stochastic dynamic models for different aggregation levels and types of DERs (air-conditioners, water-heaters, batteries, PV inverters). The aggregate model of VB is developed to predict the short term (15 minutes, $< 10\%$ RMSE) and long term (1-2 hours, $< 15\%$ RMSE) kW flexibility depending on the accuracy of the forecasts and measurement data, while also satisfying local consumer energy requirement within the STL. We characterize the aggregated VB model for the STL as

$$
\begin{aligned}
&\dot{B}(t) = -aB(t) - P^{\mathrm{b}}(t)\,, \quad B(0) = B_0 \\
&B(t) \in \left[C^-(t), C^+(t)\right] \\
&P^{\mathrm{b}}(t) \in \left[P^-(t),\, P^+(t)\right],
\end{aligned}
\tag{1}
$$

where B represents the virtual energy state of the VB with initial condition B_0, a is the strictly positive self-dissipation coefficient (generally very small), P^{b} is the VB's control input denoting the relative injection into the grid (above its nominal baseline power demand). The lower and upper energy and power bounds, C, P are denoted by corresponding superscripts $(.)^-, (.)^+$. Thus, this aggregated VB is represented by the set of parameters

$$
\Phi = \left(a, B_0, C^-, C^+, P^-, P^+\right),
$$

which must be computed to characterize the VB. Note that the aggregated VB model (1) guarantees that for every set of 'admissible' trajectories $P_i^{\mathrm{dev}}(t)$ for each of individual device $i = 1, \ldots, N$, the aggregated power trajectory $P^{\mathrm{b}}(t)$ is also admissible for the VB at the service transformer level.

In this project, we proposed two complementary, novel methods for parameterizing the VB model: 1) optimization-based binary search for finding $[P^-, P^+]$); and 2) learning-based

15

framework for the other parameters (a, B_0, C^-, C^+). The learning-based framework was shown to be more versatile via the use of transfer learning. For details on the learning-based methodology, please see [30, 32], which are summarized next.

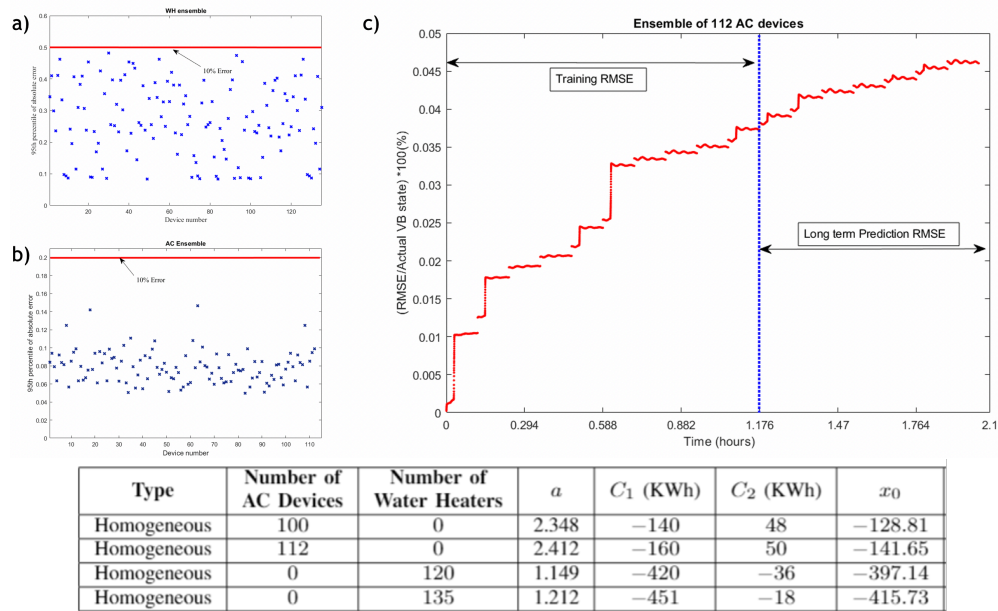| Type	Number of AC Devices	Number of Water Heaters	a	C_1 (KWh)	C_2 (KWh)	x_0
Homogeneous	100	0	2.348	-140	48	-128.81
Homogeneous	112	0	2.412	-160	50	-141.65
Homogeneous	0	120	1.149	-420	-36	-397.14
Homogeneous	0	135	1.212	-451	-18	-415.73

Figure 3: Validation of learning-based VB model.

The transfer learning-based deep network framework worked well for dynamically updating the VB parameters such as self-dissipation (a) and capacity bounds (C^-, C^+) for ensembles of flexible thermostatic loads, from the available device-level measurements. Fig. 3 shows the accuracy in estimating B_0 and forecasting using a transfer learning-based, deep network framework. Plots a) and b) (on the left) show that a stacked auto-encoder (SAE) architecture is able to accurately encode-decode device states with less than 10% error, where error is w.r.t. 10% of AC's and electric water heater's (EWH's) allowable ranges of $\pm 2F$ and $\pm 5F$, respectively). Plot c) (on the right) shows flexibility forecasting errors of less than 0.5% more than 1 hour out. The bottom table shows the VB parameters from four different DER ensembles that have been tested with this proposed deep network based framework. This framework is generalizable and can be extended for other ensembles (mix of different type of DERs) and to changing population using a transfer-learning Net2Net methodology developed in this project. To ensure that the forecast flexibility from the VB model achieves target accuracy, we leveraged a long-short-term-memory (LSTM) network with a two-stage training process. Finally, we introduced a convolution based LSTM network for forecasting the VB state evolution.

Milestone delivered:

- M (ST-1.1.3) Aggregate model of DER is developed to predict (with RMSE) the short term (15 minutes) and long term (1-2 hours) flexibility depending on the accuracy of the forecasts and measurement data, while also satisfying local energy requirements in the STL.

Task 1.2 - Real-time Coordination of DERs with Tracking Controller

The goal of this task in Year 2 was to improve the STL's ability to track a power reference set-point in real-time (M1.2.1) under realistic stochastic PV and load conditions (M1.2.2), thereby improving reliability. Achieving this goal is necessary for the success of the FOL (and, correspondingly, the GML) and for system reliability. To complete this objective, we first tested the STL-DER dispatch (i.e., the disaggregator in Fig. 4 and detailed in [31, 36]) in simulation on step and ramp up/down reference signals and showed that tracking errors for a diverse fleet of 200 ACs and 100 EWHs were less than 3-7% with errors closer to 7% when the reference signals decreased. This was much lower than the target value of 15% and indicated that STL could accurately dispatch smart, responsive DERs every second to a desired active power set-point. Furthermore, we achieved real-time root-mean-square (RMS) tracking error for step and ramp responses at the GML below 3.5%, which is much lower than the target value of 10%.
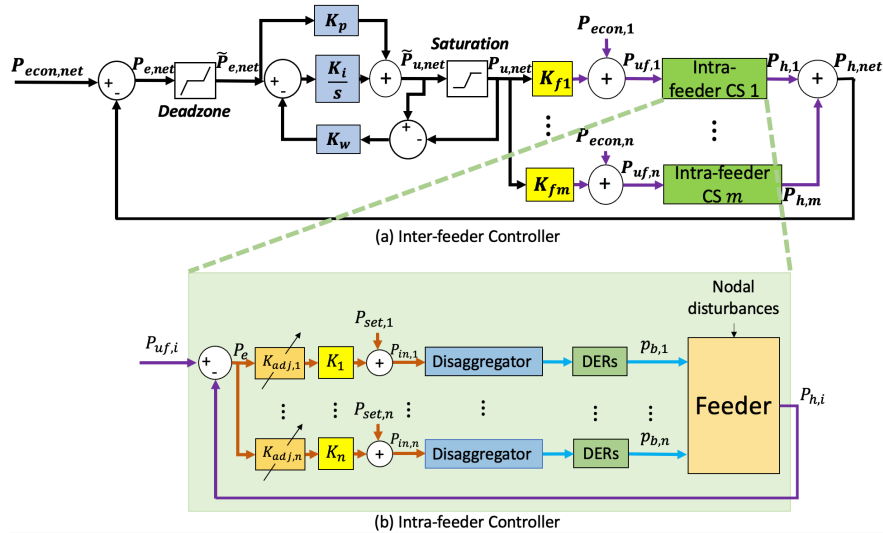

Figure 4: Real Time Inter- and Intra-feeder Control Scheme

Then, based on common concepts from wide-area control in transmission, we developed a novel proportional intra-feeder and a PI inter-feeder (corrective) controller (see Fig. 4) that dynamically update VB active power set-points to track the desired economics head-node target value (i.e., reject disturbances from solar PV variability).

The inter-feeder control system mitigates large disturbances occurring within and across feeders, and is depicted in Fig. 4a. It is essentially a PI control scheme with a dead-zone and anti-windup mechanism that corrects the GML economic set-point references, $P_{econ,r}$, to the m intra-feeder control systems (Fig. 4b). The working principle of the inter-feeder controller is as follows: The sum of measured head node active powers from all feeders, $P_{h,net}$, is compared with the total economic market set-point for all feeders, $P_{econ,net}$, and the error between them is passed through a dead-zone filter and PI controller with anti-windup. Then, the control input to the rth intra-feeder control system, $P_{uf,r}$, is computed as $P_{uf,r} = K_{fr}P_{u,net} + P_{econ,r}$, where $P_{econ,r}$ is the economic set-point for the rth feeder, K_{fr}

is a scaling factor, and $P_{u,\text{net}}$ is the output of the PI controller (with appropriate limits).

The intra-feeder control scheme, on the other hand, rejects short-term disturbances (like solar PV/demand fluctuations) that enter the primary MV nodes of a feeder and maintain the FOL set-point at the feeder's head-node (i.e., substation). To control the DERs in this scheme, the only measurement required is the active power at the head-node of the feeder, which is available at the substation, e.g., via RTACs. The scheme is depicted in Fig. 4b, as a zoomed version of the green block in Fig. 4a, and, essentially, consists of a bank of proportional controllers, K_r, multiplied by certain dynamic adjustment factors, $K_{\text{adj},r}$, one to control each of the n groups of DERs in the feeder. The corrected economic reference head-node power for this feeder, $P_{uf,i}$, is calculated by the inter-feeder controller described before, and $P_{h,i}$ the head node power of the feeder. Uncontrolled nodal disturbances are assumed to enter the feeder at multiple sites, unknown to the controller. The corrected set-point for the rth set of DERs, $p_{\text{in},r}$, is obtained as $p_{\text{in},r} = K_r K_{\text{adj},r}(P_{uf} - P_h) + P_{\text{set},r}$, where $P_{\text{set},r}$ refers to the set-point provided by the FOL optimal set-point dispatcher about every minute, and $K_{\text{adj},r}$ is an adjustment factor that ensures that as the energy states of the VBs corresponding to the sets of DERs approach full capacity, the charging rate is proportionately reduced, and when the energy state becomes empty, the discharging rate is proportionately reduced (similar to standard gain scheduling). This helps to avoid a sudden step-change in power to zero when the DERs saturate (either empty or full capacity). The "disaggregators" then recast $P_{\text{in},i}$ as ON/OFF signals for individual devices using the optimization-based dispatch. In Fig. 4, substation level signals are colored black, feeder level signals are colored violet, STL level signals brown, while device level signals are colored blue.

The controllers employ the DSO's own secure communication network and state-of-the-art IEC standards and a lag-based model of the VB (to account for both energy and power dynamics associated with delays between devices being commanded by the STL the the device switching ON/OFF). Specifically, the inter-feeder PI control can be used on the feeder substation to track the GML set-point and correct inter-feeder disturbances while the intra-feeder proportional control can be used at the VBs to correct for nodal disturbances within each feeder. The controllers can be straightforwardly extended to PV power set-points as well by removing the energy-aware adjustment of the gains in the intra-feeder controller.

The controller gains can be chosen so as to ensure performance and stability and simulation results validate the effectiveness of the real-time control technique in Task 4 (please, see below). The process for choosing controller gains is described next:

Selection of Intra-Feeder Controller Gains

The intra-feeder controller gains were selected optimally using an approach similar to standard linear quadratic regulator (LQR). First, the rth set of DERs (in Fig. 4b) was modeled as a VB with a first order lag τ_r and a delay T_{dr}, with the transfer function (similar to [37] for example):

$$V(s) = \frac{e^{-T_{dr}s}}{\tau_r s + 1} \tag{2}$$

This model was formed by taking note of the following facts: i) The DERs that compose a VB turn on/off (possibly) sequentially, and there are electronic and mechanical components (e.g., relay) present inside each VB, both of which contribute to a net lag τ_r; ii) There

are communication delays (generally of the order of 200 ms) between the head node of the feeder and each VB [38, 39], and delays associated with disaggregating the control signal into device-level signals using the optimization-based approach [40]. The delays we considered in the VB model were both these types of delays lumped together. Based on typical observed server communication times and the device-level optimization solve-times, we assumed both the time delays and the lags to be less than 200 ms for design.

To design the proportional gains, we assume that the feeder is affected by nodal injections that are stochastic. This is reasonable since solar PV and demand fluctuations are typically random. The objective is then to reduce the effect of these injections on deviating the head-node power from the economic reference. Alternatively, we can treat the reference signal itself as stochastic and reduce the standard deviation of the tracking error. To do that, first, the system is linearized by linearizing the AC power flow equations about an operating point set by the FOL. This done by finding the sensitivity of the head node active power of the feeder to the active power injection at the particular nodes where the DERs are situated. The time-delays in the transfer function (2) were ignored during the computation of the gains but were accounted for by designing gains in such a way that the gain-crossover frequency of the open-loop system, or the bandwidth of the closed-loop system (without delays), is less than $1/5T_{d,\max}$, where $T_{d,\max}$ is the maximum time delay in the system. Effectively, this ensures that the delay-free system and the delayed system behave similarly. Then, assuming that the system is excited by zero-mean wide-sense stationary Gaussian inputs, we minimize the sum of the variance of the error, P_e, denoted by $\sigma^2_{P_e}$, and a weighted sum of the variances of the control inputs to each VB, $P_{u1}, \ldots, P_{un}$, denoted by $\sigma^2_{P_{u1}}, ..., \sigma^2_{P_{un}}$ respectively:

$$\min_K \quad \sigma^2_{P_e}(K) + \sum_{r=1}^n \rho_r \sigma^2_{P_{ur}}(K), \tag{3}$$

where $K = \begin{bmatrix} K_1 & K_2 & \ldots & K_n \end{bmatrix}^\top$. Here, $\sigma_{P_e}(K)$ and $\sigma_{P_{ur}}(K)$ are related to the standard deviation of the reference via the $\mathcal{H}_2$-norm of the transfer function of the closed-loop system, and to the gains K_r through the Lyapunov equation, $A\Sigma + \Sigma A^\top + BB^\top = 0$, where A, B are system state matrices and Σ is the state covariance matrix. See [41] for details. $\rho_r > 0$ is a constant penalty parameter that we design to be inversely proportional to the power capacity of the rth VB. This penalizes power extraction from VBs that have a lower capacity to provide power output, thus resulting in a *constraint-aware* controller. In our design, we used a value of $\rho_r \approx 6$. The above nonlinear optimization problem was solved using the Broyden–Fletcher–Goldfarb–Shanno algorithm [42] in SciPy's `minimize` [43]. The solve time for optimizing each intra-feeder control system was around 100-200 ms (which is small, considering that it needs to be solved only around every 1-5 minutes if the FOL changes STL set-points or when topology changes).

Selection of Inter-Feeder Controller Gains The inter-feeder PI controller gains K_p and K_i were selected by minimizing the settling time t_s of the overall system response, subject to standard phase margin PM $> 40°$. This is done because a high phase margin ensures that the system remains robust to VB failure, while a low settling time of less than a minute ensures that any large disturbance is quickly rejected before the optimal dispatcher provides new set-points to VBs every minute. To do this, first, the overall system is linearized in

the same manner as for the Intra-feeder controller design. Then, the following optimization problem is solved to find K_p and K_i:

$$\begin{aligned} \min_{K_p, K_i} \quad & t_s \\ \text{s. t.} \quad & \text{PM} > 40° \end{aligned} \tag{4}$$

where t_s is the settling time of the entire closed-loop system due to the response to a step input applied at $\Delta P_{\text{econ,net}}$ and PM is the phase margin of the open-loop transfer function from $P_{e,\text{net}}$ to $P_{h,\text{net}}$. This nonlinear optimization problem was solved using a global minimization Basin-Hopping algorithm [44] in SciPy's `minimize` [43]. The solve time was around 5 s (which is reasonable considering that this optimization needs to be performed about every 5 min).

To penalize the extraction of power from feeders with lower capacity to provide power, the inter-feeder gains K_{fi} are chosen in proportion to the total capacity of the feeder with which they are associated. If the feeder i has a higher capacity, K_{fi} is assigned a higher value, and if it has a lower capacity, K_{fi} is assigned a lower value. Specifically, $K_{fi} = \overline{P}_i/\overline{P}$, where $\overline{P}_i$ is the power capacity of the ith feeder, and $\overline{P}$ is the total power capacity of all feeders. Also, the anti-windup gain K_w was set to unity to ensure a satisfactory performance during recovery from VB saturation. Task 4 includes validation of the above methodology for inter-layer, real-time corrective control of VB.
Milestones delivered:

- M (ST-1.2.1) Root-mean-square tracking error for step and ramp responses (after transients have subsided) over a 5-15 minute period
- M (ST-1.2.2) Root-mean-square tracking error for step and ramp responses under realistic forecast conditions (after transients have subsided) over a 5-15 minute period

Task 2: Feeder Operational Layer (FOL)

In Year 1, the goal of Task 2 was two-fold: 1) develop proof-of-concept distribution system state estimation (DSSE) and 2) develop deterministic OPF formulation for unbalanced AC distribution feeders. The reason to pursue the DSSE was to endow the OPF with model feedback to enable a simplified, but accurate predictive formulation for optimizing the dispatch of continuous VB and PV inverter assets (inner-loop, M2.1.3). In addition, we developed a novel voltage-positioning framework to maximize voltage margins on a slower timescale with legacy mechanical assets (M2.1.4). In Year 2, Task 2 shifted focus from deterministic to stochastic formulations to account for intra-hourly solar PV forecasting errors, thereby improving reliability.

The key challenge with Task 2 was the fact that the underlying physics for an unbalanced distribution network required development of new optimal power flow routines and methods. The model of an unbalanced feeder is introduced next and used in both DSSE and OPF routines presented further below.

Modeling unbalanced feeders

Given a radial, 3-phase feeder with nodal set $\mathcal{N} = \{1, 2, \ldots, N\}$ of which a subset have DERs attached $\mathcal{G} = \{1, 2, \ldots, G\} \subseteq \mathcal{N}$, and set of branches $\mathcal{L} = \{1, 2, \ldots, L\} = \{(m, n)\} \subset (\mathcal{N} \times \mathcal{N})$, the physics of 3-phase AC power flows are given by the standard equations [45]:

$$0 = W_n(t) - W_m(t) + (S_l(t)Z_l^* + Z_l S_l(t)) - Z_l I_l(t)Z_l^* \quad \forall l \in \mathcal{L} \tag{5a}$$

$$0 = \mathrm{diag}(S_l(t) - Z_l I_l(t) - \sum_p S_p(t)) + S_n^{\mathrm{net}}(t) \quad \forall l \in \mathcal{L} \tag{5b}$$

$$\begin{bmatrix} W_n(t) & S_l(t) \\ S_l(t)^* & I_l(t) \end{bmatrix} = \begin{bmatrix} V_n(t) \\ i_l(t) \end{bmatrix} \begin{bmatrix} V_n(t) \\ i_l(t) \end{bmatrix}^* \quad \forall l \in \mathcal{L} \tag{5c}$$

$$0 = \mathrm{real}\{S_n^{\mathrm{net}}(t) - S_n^{\mathrm{S}}(t) + S_n^{\mathrm{L}}(t)\} - P_n^{\mathrm{b}}(t) \quad \forall n \in \mathcal{G} \tag{5d}$$

$$0 = \mathrm{imag}\{S_n^{\mathrm{net}}(t) - S_n^{\mathrm{S}}(t) + S_n^{\mathrm{L}}(t)\} \quad \forall n \in \mathcal{G} \tag{5e}$$

In (5), (5a) relates the voltage drop in the network with the branch power flows, (5b) represents the power balance equation at each node which ensures that the power entering a node equals the power leaving, and (5c) is the non-linear power flow constraint that relates voltages and currents to new matrix variables $W_n(t)$, $I_l(t)$ and $S_l(t)$. In (5d) and (5e), the active and reactive nodal power balance equations are defined.
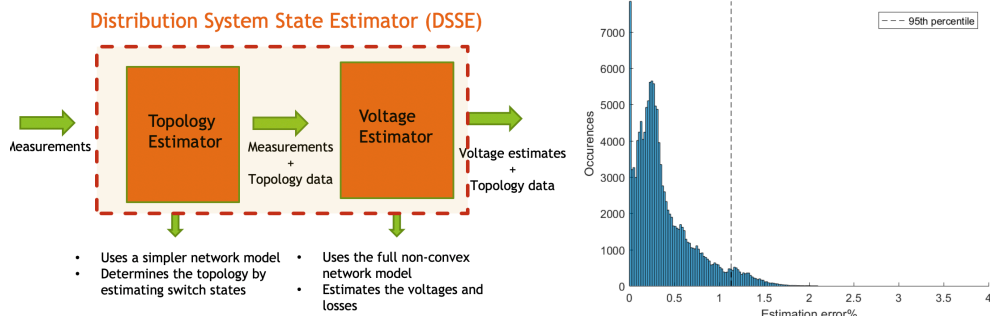

Figure 5: Distribution System State Estimation. (Left) The novel DSSE supports the FOL and enabled model-based feedback for the OPF-based dispatch of VB and PV inverters. The DSSE problem consist of a Voltage Estimator (DSSE-VE, M2.1.1) and Topology Estimator (DSSE-TE, M2.2.1) to decompose the full mixed-integer nonconvex estimation problem into two simpler sub-problems. (Right) The estimation error from deterministic DSEE-VE applied to the IEEE 123-node test network showing that 95% of voltage estimates have errors below 1.5%.

Task 2.1 - Operation & Real-time Coordination of Deterministic FOL

The goal of Task 2.1 is two fold: 1) develop a DSSE methodology for unbalanced networks to detect topology changes and estimate network states (e.g., voltages, currents, and line losses) and 2) use the line losses to enable scalable OPF formulation in FOL for dispatching controllable grid resources. To achieve the former, we developed a DSSE algorithm as a nonlinear non-convex weighted least-square optimization problem that fuses measurements

21

of voltage magnitude (e.g., from μPMU or DERs or AMI) and voltage phase (e.g., from μPMU) at about 10% of nodes with SCADA (for power-flows, voltage magnitude), AMI (power injections), and historical data (e.g., estimated load patterns) to estimate voltage phasors at **all** nodes. The DSSE voltage estimation problem with mixed measurements is given by

$$\hat{V} = \arg\min_V \sum_{i \in M_S} \left(h_{S_i}(V) - \hat{S}_i\right)^2 \sigma_S^{-1} + \sum_{i \in M_v} \left(h_{V_i}(V) - V_i^m\right)^2 \sigma_i^{-1} \tag{6}$$
$$+ \sum_{i \in M_{|v|}} \left(h_{|V_i|}(V) - |V_i|^m\right)^2 \sigma_{|i|}^{-1}$$

subject to: $|V| \in [0.5, 1.5], \ \angle V \in [-\pi, \pi],$

where functions $h_{(.)i}(V)$ map estimated voltages V to (pseudo) measured parameter (.) at node i and $S, V^m, |V|^m$ represent noisy pseudo-measurement data from AMI/SCADA (with high-variance), real-time voltage phasor, and real-time voltage magnitude data (with low variance), respectively.

- For the deterministic case of the DSSE's Voltage Estimator (see Fig. 6), we tested the algorithm on two test-feeders: 1) a single-phase 33-bus radial distribution feeder (MAT-POWER testcase), and 2) an IEEE 13-bus three-phase unbalanced distribution feeder. The node voltage estimation errors were within 1-3% for over 95% of the samples for a summer month period, which exceeds the 5% spec set. The GML's power reference for the feeder is provided to FOL, which employs the DSSE to provide estimated states of the network. These states are used to inform the FOL's inner-loop OPF formulations of line losses that enable accurate tracking of said reference via DSSE's feedback.
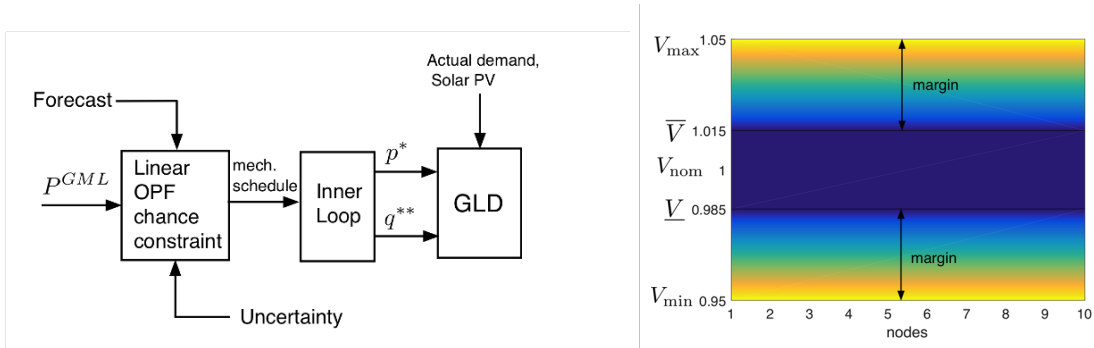

Figure 6: Voltage positioning in the FOL. (Left) The FOL's outer-loop (OL) is cast as a voltage positioning (VP) problem, which employs a convex model to maximize voltage margins given an expected economic feeder power target from the GML and validated with GridLab-D (GLD). (Right) Voltage margins are represented as the minimum distance from a nominal range $[\underline{V}, \overline{V}]$ to $V_{\min}$ and $V_{\max}$.

- Before optimizing VBs and PV inverters with the FOL's inner-loop, we need to schedule discrete assets first as shown in Fig. 6. This is accomplished with the FOL's novel voltage positioning (VP) outer loop formulation that solves a multi-period (3-12 hourly periods ahead) mechanical asset scheduling problem. The VP formulation employs a linearized

22

three-phase feeder model that maximizes voltage margins (i.e., robustly position voltages) while tracking a headnode power reference while minimizing the utilization of flexible VB and PV inverter resources. The VP formulation is given by the below:

$$\min_{V,q^{\mathrm{pv}},p^{\mathrm{vb}}} (P_0 - P_0^{\mathrm{GML}})^2 + (Q_0 - Q_0^{\mathrm{GML}})^2 + \rho \sum_i \left((p_i^{\mathrm{vb}})^2 + (q_i^{\mathrm{pv}})^2\right) + \rho_V \sum_i V_{\mathrm{s},i} \tag{7a}$$

$$\text{s.t.} \quad \text{linear power flow relations (LP)} \tag{7b}$$
$$\text{branch power flow limits (LP)} \tag{7c}$$
$$\text{discrete/legacy asset constraints (McCormick, MISOCP)} \tag{7d}$$
$$\text{continuous/responsive asset constraints (SOCP)} \tag{7e}$$
$$-V_{\mathrm{s},i} + \underline{V}_i \le V_i \le \overline{V}_i + V_{\mathrm{s},i} \tag{7f}$$
$$V_{\mathrm{min},i} \le V_i \le V_{\mathrm{max},i} \tag{7g}$$
$$V_{\mathrm{s},i} \ge 0 \tag{7h}$$

where a linear power flow is employed which is suitable due to the longer prediction horizon and slower (hourly) timescale. The first two terms in the objective (7a) track the GML's active and reactive power setpoints at the head-node $P_0^{\mathrm{GML}}, Q_0^{\mathrm{GML}}$. The third term minimizes the use of reactive power from solar PV and VB resources $q_i^{\mathrm{PV}}, p_i^{\mathrm{VB}}$. The last term penalizes the voltage slack $V_{\mathrm{s},i}$ to maximize voltage margins. The parameters ρ and ρ_V are chosen so as to achieve a trade-off between utilizing flexibility to position voltage close to nominal or utilize the voltage slack and prioritize the flexible resources for the FOL's inner loop. The discrete legacy assets represent bilinear constraints (MI-NLP) that can be relaxed with McCormick to MISOCP, which is also the formulation for continuous responsive assets, like PV inverters. In addition, to make the VP formulation tractable for larger networks with more discrete assets, VB flexibility p_i^{VB} can be omitted from the VP problem, which removes the VB's temporal coupling of constraints.

In Year 1, we had to validate the VP performance for a network with >100 nodes to within 5% of optimal solution in less than 300 seconds with default mixed-integer solver settings while satisfying all constraints. To accomplish this, we reformulated the VP objective using convex optimization techniques to create a MISOCP formulation. The novel formulation allows the voltages to deviate from nominal (e.g., 1.0pu) by a pre-defined narrow range (e.g., ±0.02pu) and penalizes solutions that are beyond that level (i.e., the voltage margin is now a priced resource in the FOL outer-loop VP problem). Since the use of reactive power assets helps manage voltages, there is a natural trade-off between voltage deviations from nominal and the use of reactive power resources, so we priced reactive power resources as well. We capture this trade-off in the VP by considering the sensitivity of voltage deviations and reactive power injections in designing a "narrow-enough" range of acceptable deviations. In year 1, we validate the formulation on IEEE-123 node network and the MISOCP solved in less than 70 seconds with 0% constraint violations and with less than a 5% optimality gap, which met the goals and satisfied the reliability metrics.

- The mechanical schedule is supplied to the FOL's novel inner loop (IL), which eliminated discrete variables and the IL can then solve a continuous unbalanced AC OPF to optimize the dispatch of the VBs to track the GML's supplied power reference. This is accomplished by solving a multi-period (ten to thirty 1-5-minute periods) OPF dispatch to account for temporal coupling induced by energy dynamics in the VBs. It is important that the solution is good (i.e., close to optimality or $< 5\%$ optimality gap) and physically meaningful to ensure that the implemented dispatch does not violate ANSI limits on voltages, thereby maintaining system reliability. In addition, it should be computationally efficient since we would like to repeatedly solve IL OPF every minute or so to update VB set-points given the timescale of solar PV variability. Thus, a novel two-stage SOCP-NLP formulation was developed for the FOL's inner loop to perform set-point optimization for VBs and PV inverters within a feeder.

Note that the SOCP solution may not be physically realizable due to the non-zero duality gap in convex relaxation, so a warm-start NLP optimization is initialized with the SOCP solution and solved for reactive power set-points. Test simulations are conducted on 3-phase model of IEEE 123-node test system with validation performed using GridLab-D. The simulation results confirm the NLP optimization solution by producing matching results. The SOCP-NLP optimization algorithm takes on average about 11 seconds to solve in total, which is well below the 60 sec solve time requirement. The optimality gap between the SOCP and NLP was found to be less than 5%. As the SOCP optimal value is a lower bound to the global optimum, the obtained solution will be within 5% of the global optimum. From validation with GridLab-D (GLD), the obtained optimal solution matches with the simulation results and is found to be within the feasibility bounds. This preliminary evidence was important for the project as it showed technical feasibility of the FOL's unbalanced OPF with satisfaction of reliability metrics.
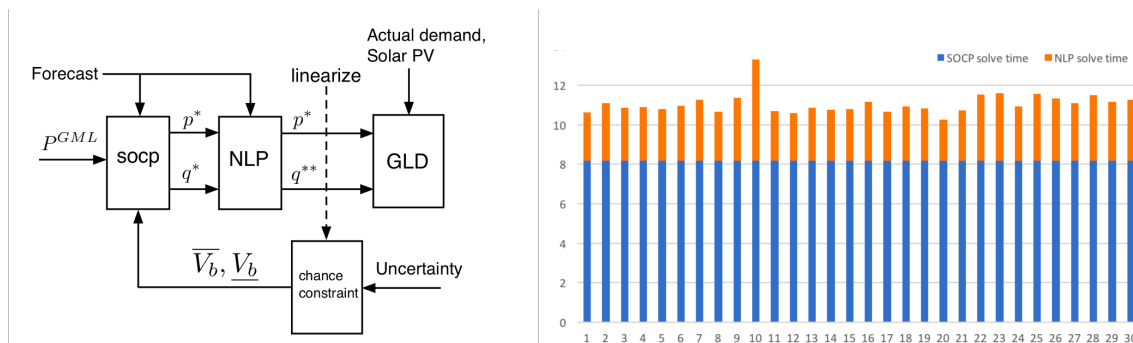

Figure 7: (Left) The FOL's inner-loop (IL) is cast as a two-stage SOCP-NLP problem, where the SOCP handles multi-period relaxed version of the ACOPF and passes the solution to the NLP to warm-start but fixes the NLP's VB active power set-points (p^*), so the NLP can focus on optimizing the the reactive power set-points (q^{**}) of PV inverters to keep voltages within limits. Note that the chance constraint is the outcome of Year 2 work on robust extension and is described later. (Right) The new SOCP-NLP combination ensures efficient computation and guarantees physical admissibility of the solution.

Milestones delivered:
- M (ST-2.1.1) State Estimator voltages during a one-month period in a summer month for averaged per-phase values

24

- M (ST-2.1.3) Solve multi-period (12-24 hourly periods) mechanical asset scheduling problem for three-phase feeder model with >100 nodes (each with a parametrized virtual battery representing around 10-20 devices) to within 5% of optimal solution with default GUROBI (or open-source BONMIN) mixed-integer solver while satisfying all constraints.
- M (ST-2.1.4) Solve multi-period (ten to thirty 1-5-minute periods) optimal STL element dispatch to within 5% of optimal solution on a standard laptop with default GUROBI (or suitable open-source solvers) settings in suitable time and verify that the optimal dispatch is physically realizable with respect to relevant grid constraints through physical simulation of solution on three-phase unbalanced system.

Task 2.2 - Uncertainty-aware optimization for FOL

For Task 2.2, Year 2 generally focused on robustness against uncertainty in terms of the network topology (for the DSSE) and solar PV forecast (for the FOL's OPF). This ensures a robust OPF framework in a practical setting.

- For the DSSE to remain robust to uncertainty in the feeder topology, we needed to develop the DSSE-TE shown in Fig. 5(Left). The DSSE-TE employed a linearized, 3-phase power flow model and a known set of possible topologies (since the switch locations are known *a priori*). Since the possible admittance matrices were known before hand, a time-varying load profile was combined with the different network topologies to create a set of scenarios on which the topology/voltage estimator is validated. Note that the number of possible topologies is limited for a single feeder, which keeps the number of scenarios small. A sensor profile was identified for each of the test feeders which detects topology changes with 100% accuracy (See Fig, 8(Top)) and it could be shown that one voltage measurement per unique island is sufficient to guarantee perfect outage detection. Since the DSSE-TE performed rather well, the combined topology and voltage DSSE achieved estimation errors below 0.5% for 95% of all voltage magnitudes for three different test-systems shown in Fig. 8, which satisfies the project's requirement of $\geq 99\%$ observability. Note that since the number of switches is generally much smaller than the number of nodes and we likely just need the same number of sensors (located near the switches and measuring voltage and P/Q power flows), the formulation can scale well.

- In Year 2, we wanted to focus on robustifying both the FOL's inner and outer loops' OPFs to account for solar PV, thereby improving reliability. However, the FOL's outer loop that solves a mechanical asset MIP scheduling problem to maximize voltage margins is already robust by nature of maximizing voltage margins. Thus, it became clear from simulation results, see for example Fig 9(top), that only the inner-loop needed to be made robust against uncertainties.

- Based on the experience with the FOL's outer-loop, we decided to add chance constraints to the FOL's inner loop OPF formulation as shown in Fig. 7. The methodology should ensure that any solution be physically realizable on 3-phase feeder model with voltage and branch constraints. Voltage or current violations should be small ($< 1\%$, $< 10\%$, respectively for voltage and currents) and strictly temporary (< 10 minutes). The approach we took was to use the DSSE to determine the network's state and from that
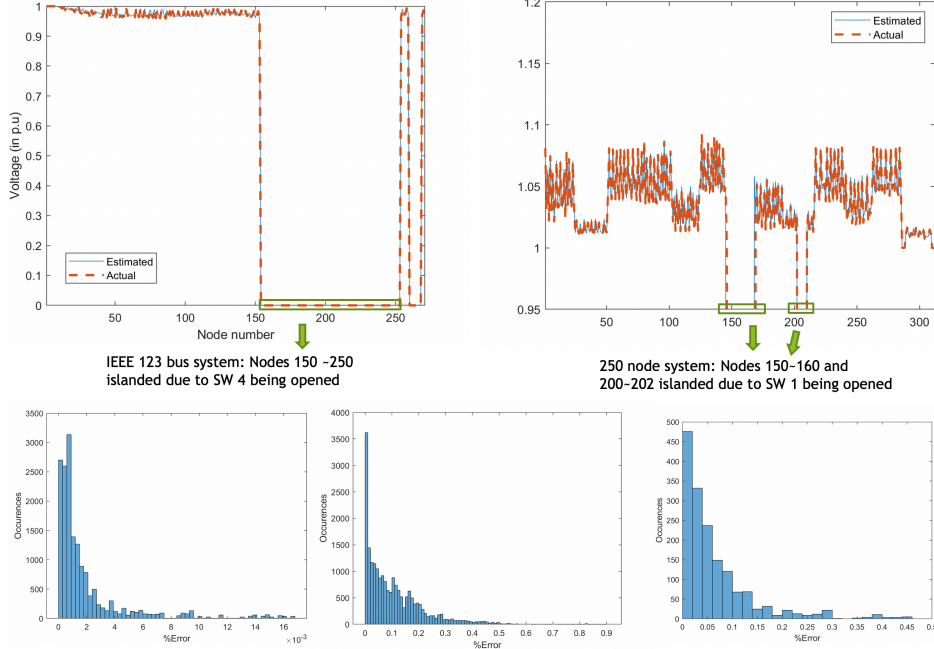
25

Figure 8: (Top) DSSE-TE detected topology with 100% accuracy in both left and right network scenarios. (Bottom) Combined DSSE-TE-VE voltage estimates with less than 0.5% error for 95% of estimates.

estimate, linearize the 3-phase OPF and add additional linear constraints that effectively tightens the voltage bounds. This approach is pragmatic but a little less elegant than the literature on stochastic OPF. However, the approach is computationally effective and does not perturb the two-stage SOCP+NLP formulations.

- We can now formulate the final robust, multi-period SOCP optimization problem solved in the FOL. First, consider the objective function that tracks the GML's computed economic power targets for the head-node (active P^{GML}), total VBs (active R_f), and total solar PV (active P_f^g and reactive Q_f^g) and reduces total line losses, if possible, with ϵ small.

$$
f_1(x) := \sum_{t \in \mathcal{T}} \left(\left(L_1(t) + P^{\mathrm{GML}}(t) - \sum_{n \in \mathcal{N}} \mathrm{real}\{S_n^{\mathrm{net}}(t)\} \right)^2 + \alpha \left(R_f(t) - \sum_{n \in \mathcal{N}} P_n^{\mathrm{b}}(t) \right)^2 \right.
$$
$$
\left. + \beta \left(P_f^{\mathrm{g}}(t) - \sum_{n \in \mathcal{N}} \mathrm{real}\{S_n^{\mathrm{S}}(t)\} \right)^2 + \gamma \left(Q_f^{\mathrm{g}}(t) - \sum_{n \in \mathcal{N}} \mathrm{imag}\{S_n^{\mathrm{S}}(t)\} \right)^2 + \epsilon \sum_{l \in \mathcal{L}} \mathbf{1}^\top \mathrm{diag}(R_l \circ I_l(t)) \right).
$$

The first term in $f_1(x)$ represents the FOL's tracking of the GML's computed feeder head-node power reference P^{GML} with $L_1(t) = L_0(t) + \sum_{n \in \mathcal{N}} \zeta_n \Delta p_n(t)$ being a first-order approximations of the total feeder line losses, $L_0(t)$ is the loss estimated for the operating point at time t, and $\zeta_n \Delta p_n(t)$ represents the change in total feeder losses due to the change in active power injection at node n. The factors ζ_n represent the sensitivity in feeder losses due to changes in active power injections and are similar to the power transfer distribution factors (PTDFs) that are often used in transmission system analysis [47]. The
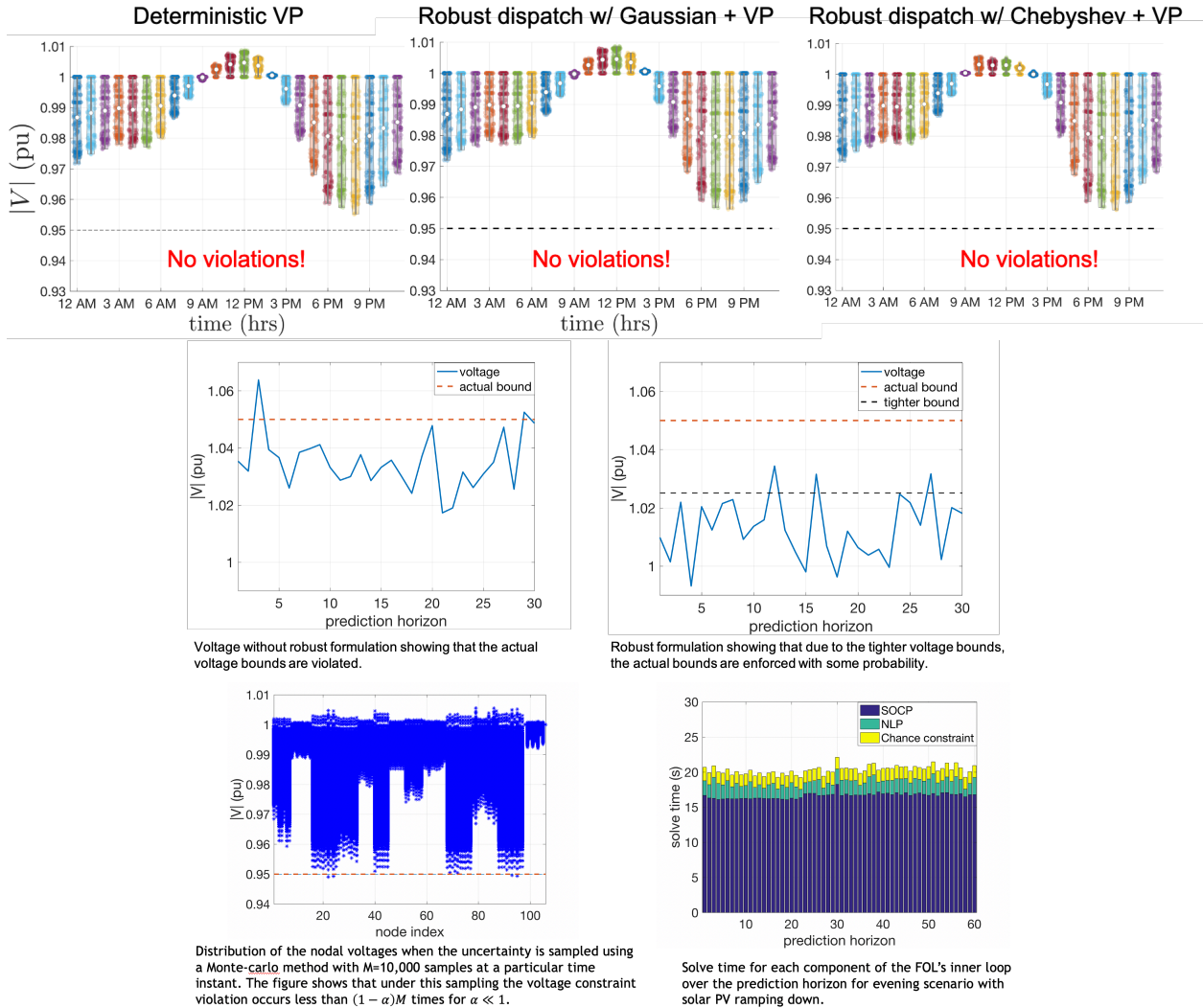
Figure 9: Robust SOCP+NLP for FOL. (Top row) Comparing the deterministic VP formulation from ([7]) (Top left) against two different robust formulations (under assumed Gaussian and Unimodular forecast error assumptions, see [46]) for a 261-node reduced ORU network for a full day with peak solar PV generation around noon. Clearly, all are robust to the uncertainty. So there is no reason to change the deterministic VP formulation. (Middle Left) For the 261-node reduced network, we see Deterministic inner-loop voltage profile; (Middle right) Voltage profile for the robust inner-loop with tighten bound, which is around 0.02pu in this case; (Bottom left) Nodal voltages over 60 simulated time-steps show that there are little to no voltage violations and that the robust formulation works; (Bottom right) solve times are consistently fast over a 60-timestep horizon and significantly shorter than the 60s that are required in SOPO (Bottom row).

Table 1: Control variables used in the FOL and GML formulations.

Variable type	Variables
FOL control variables	P_n^{b} (VB), S_n^{S} (PV), $V_{\mathrm{v},n}^+$, $V_{\mathrm{v},n}^-$
GML control variables	P^{GML}, R_f (VB), P_f^{g} (PV), Q_f^{g} (PV)

second term ensures tracking of the GML's provided VB power reference R_f for feeder f. The third term tracks the GML's provided solar PV power reference P_f^{g}, the fourth term tracks the GML's provided reactive power reference Q_f^{g} and the final term additionally minimizes feeder losses. This objective is used to formulate the robust SOCP:

$$\min_{x} \quad f_1(x) + \eta \sum_{t \in \mathcal{T}} \sum_{n=1}^{N} \mathbf{1}^{\mathbf{T}} (V_{\mathrm{v},n}(t)^+ + V_{\mathrm{v},n}(t)^-) \tag{8a}$$

s.t.

$$(5a), (5b), (5d), (5e), \tag{8b}$$

$$B_n(t+1) = B_n(t) - P_n^{\mathrm{b}}(t)\Delta t \qquad \forall n \in \mathcal{G}, \tag{8c}$$

$$\left\| \frac{2W_n(t)(i,j)}{W_n(t)(i,i) - W_n(t)(j,j)} \right\|_2 \leq W_n(t)(i,i) + W_n(t)(j,j), \tag{8d}$$

$$\left\| \frac{2I_l(t)(i,j)}{I_l(t)(i,i) - I_l(t)(j,j)} \right\|_2 \leq I_l(t)(i,i) + I_l(t)(j,j), \tag{8e}$$

$$\left\| \frac{2S_l(t)(i,j)}{W_n(t)(i,i) - I_l(t)(j,j)} \right\|_2 \leq W_n(t)(i,i) + I_l(t)(j,j), \tag{8f}$$

$$|\mathrm{diag}(S_l(t))| \leq \overline{L}_{\mathrm{b},l}(t, \alpha_{\mathrm{L}}, \Sigma) \qquad \forall l \in \mathcal{L}, \tag{8g}$$

$$\underline{V}_{\mathrm{b},n}(t, \alpha_{\mathrm{v}}, \Sigma) - V_{\mathrm{v},n}^-(t) \leq \mathrm{diag}(W_n(t)) \leq \overline{V}_{\mathrm{b},n}(t, \alpha_{\mathrm{v}}, \Sigma) + V_{\mathrm{v},n}^+ \ \forall n \in \mathcal{N}, \tag{8h}$$

$$|S_n^{\mathrm{S}}(t)| \leq \overline{S}_{\mathrm{b},n}(t, \alpha_{\mathrm{s}}, \Sigma) \qquad \forall n \in \mathcal{G}, \tag{8i}$$

$$B_{\min,n} \leq B_n(t) \leq B_{\max,n} \qquad \forall n \in \mathcal{G}, \tag{8j}$$

$$P_{\min,n} \leq P_n^{\mathrm{b}}(t) \leq P_{\max,n} \qquad \forall n \in \mathcal{G} \tag{8k}$$

for all $t \in \mathcal{T}$, where $V_{\mathrm{v},n}(t)^+$ and $V_{\mathrm{v},n}(t)^-$ represent the slack variables that are added to ensure persistent feasibility for the upper and lower voltage bounds, respectively, and with $\eta \gg 1$. Inequalities (8i),(8j), and (8k) bounds the apparent power of solar PV inverters, state of charge (SoC), and active power dispatch, respectively. The relation between the battery SoC and VB power is given by (8c) and (8d)-(8f) are a convex relaxation of the nonlinear (5c). The α_{L}-robust bound for apparent line flows is given by $\overline{L}_{\mathrm{b},l}(t, \alpha_{\mathrm{L}}, \Sigma) := S_{\max,l} - \lambda_{\mathrm{L}}(\alpha_{\mathrm{L}}, \Sigma, S_l(t)^*)$, while the α_{v}-robust voltage bounds are given by $\overline{V}_{\mathrm{b},n}(t, \alpha_{\mathrm{v}}, \Sigma) := V_{\max,n}^2 - \lambda_{\mathrm{v}}(\alpha_{\mathrm{v}}, \Sigma, W_n(t)^*)$, $\underline{V}_{\mathrm{b},n}(t, \alpha_{\mathrm{v}}, \Sigma) := V_{\min,n}^2 + \lambda_{\mathrm{v}}(\alpha_{\mathrm{v}}, \Sigma, W_n(t)^*)$. Similarly, apparent solar inverter power bounds can be made tightened as $\overline{S}_{\mathrm{b},n}(t, \alpha_{\mathrm{s}}, \Sigma) := G_{\max,n} - \lambda_{\mathrm{s}}(\alpha_{\mathrm{s}}, \Sigma, S_n^{\mathrm{S}*}(t))$. The variable types used in the formulation are presented in Table 1. Note that the bounds are tightened by entity $\lambda_{\mathrm{Y}}(\alpha_{\mathrm{Y}}, \Sigma, Y^*) := f^{-1}(1 -$

$\alpha_Y)||\Gamma_Y\Sigma^{1/2}||_2$ which shows that the tightening depends on both the operating point Y^* and the so-called safety factor function $f^{-1}(1-\alpha_Y)$, which is defined by the acceptable probability level. The safety-factor function for the unimodal distribution is bounded by a tight inner analytical approximation:

$$f^{-1}(1-\alpha_Y) < \left(\frac{1-\alpha_Y}{e\alpha_Y}\right)^{1/1.95}.$$

For details on α and λ, please see [46, 35].

- For the robust NLP formulation in the FOL, we have the following objective function, which takes as input the solution from the SOCP and minimizes:

$$f_2(x(t)) := (Q_f^g(t) - \sum_{n \in \mathcal{N}} \text{imag}\{S_n^S(t)\})^2 + \epsilon \sum_{l=1}^{L} \mathbf{1}^T \text{diag}(R_l \circ I_l(t)),$$

and only optimizes over the FOL's controllable reactive power set-points and $P_n^{b*} \in \mathcal{R}^{|\phi|}$ is the optimal active power injection of the VB at node n obtained from the SOCP.

- This gives us the following NLP formulation:

$$\min_x f_2(x(t)) + \eta \sum_{n=1}^{N} \mathbf{1}^T \left(V_{v,n}(t)^+ + V_{v,n}(t)^-\right) \tag{9a}$$

$$\text{subject to: } (5a) - (5e) \tag{9b}$$

$$(P_n^{b*})^2 + (q_n^b(t))^2 \le H_{\max,n}^2 \qquad \forall n \in \mathcal{G} \tag{9c}$$

$$|\text{diag}(S_l(t))| \le \overline{L}_{b,l}(t, \alpha_L, \Sigma) \qquad \forall l \in \mathcal{L} \tag{9d}$$

$$\underline{V}_{b,n}(t, \alpha_v, \Sigma) - V_{v,n}^-(t) \le \text{diag}(W_n(t)) \le \overline{V}_{b,n}(t, \alpha_v, \Sigma) + V_{v,n}^+(t) \ \forall n \in \mathcal{N} \tag{9e}$$

$$|S_n^S(t)| \le \overline{S}_{b,n}(t, \alpha_s, \Sigma) \qquad \forall n \in \mathcal{G} \tag{9f}$$

where (5a)-(5e) represents the nonlinear power flow equations and (9c) represents the VB apparent power constraint with $P_n^{b*} \in \mathcal{R}^{|\phi|}$ being the optimal active power injection of the VB at node n obtained from the stochastic SOCP (8). Thus, the FOL's inner loop is the combination of the robust, multi-period SOCP formulation in (8) and the robust, time-decoupled NLPs in (9).

- In Fig. 9, the robust SOCP-NLP performance is indicative of scale and completes deliverable.

Milestones delivered

- M (ST-2.2.1) Maintain high-level of observability under unexpected sudden changes in the network, due to line switching, faults and/or outages on small network developed in ST-4.1.4.

- M (ST-2.2.2) Solve multi-period (12-24 hourly periods) mechanical asset MIP scheduling problem to within 5% of optimal solution on a standard laptop while accounting for stochastic net-loads in the small-case system developed in subtask 4.1.4. This involves at least 50 three-phase nodes for the feeder.
- M (ST-2.2.3) The solution should be physically realizable on unbalanced, realistic feeder model of more than 250 three-phase nodes with voltage and branch constraints. Voltage or current violations should be small ($< 1\%$, $<10\%$, respectively for voltage and currents) and strictly temporary.

Task 3: Grid Market Layer (GML)

The goal of the GML is to optimize flexibility of distribution-level aggregated DERs to jointly participate in the TSO-level energy and ancillary service markets. This determines the optimal aggregate interactions with wholesale energy and ancillary markets as well as feeder-level set-points for the FOL to track. In particular, GML seeks to reduce the energy procurement cost in the energy market and obtain revenue in the ancillary service market, with an optional function to simultaneously reduce peak demand. The GML also accounts for the loss due to solar curtailment to encourage solar usage.

The initial idea for Year 1 was to decompose the GML into fast and slow timescales to account for different markets, however, the efficiency of the deterministic formulation (see objective function in Fig. 10(Top)) did not necessitate the decomposition, so the GML remained as one multi-timescale optimal dispatch of feeder resources. We also initially considered a radial transmission-substation transformer bank-feeder network of feeders as in Fig. 10(Bottom-right), however, in Year 3 this was reformulated as a meshed network of feeders.

Tasks 3.1: Formulate and perform joint economic dispatch and regulation problem for feeders

The utility can coordinate feeders' flexible resources and use this flexibility to participate in real-time or ancillary services markets. By participation, we mean they can either sell or buy electricity to/from the real-time market and/or participate in an ancillary service market, specially by providing reserve services. For each feeder we consider two potential source of real power updates: (i) Solar generation (or power response) and (ii) storage from VBs. Outcome was presented at a conference [48] to complete Year 1 GML deliverables.

The main market signals for the GML include both wholesale energy and ancillary service market prices. The energy market usually operates in a two-settlement manner and clears transactions at two timescales with respective prices, i.e., day ahead with day-ahead/forward price and real-time, usually 5 minutes ahead, with real-time/spot price. We assume the clearing times of the ancillary service market coincide with the real-time market on a 5-minute basis, enabling co-optimized cross-market participation. Further, the GML is assumed to be a price taker, i.e., has no significant effect on prices.

- *Day-Ahead Market*: The day-ahead market runs for each hour of the next day simultaneously. The GML determines *optimal hourly procurement of energy* in the day-ahead market based on *predicted hourly prices* and feeder specifications subject to uncertainties

$$\min \quad \sum_{t=1}^{T} \delta_t \left(\lambda^{\mathsf{da}}(t) P^{\mathsf{da}}(t) + \lambda^{\mathsf{rt}}(t) \left(P_0(t) - P^{\mathsf{da}}(t) \right) - \alpha(t) P_{\mathsf{rsrv}}(t) + \sum_f f_{f,t}(P_f^g(t)) \right)$$
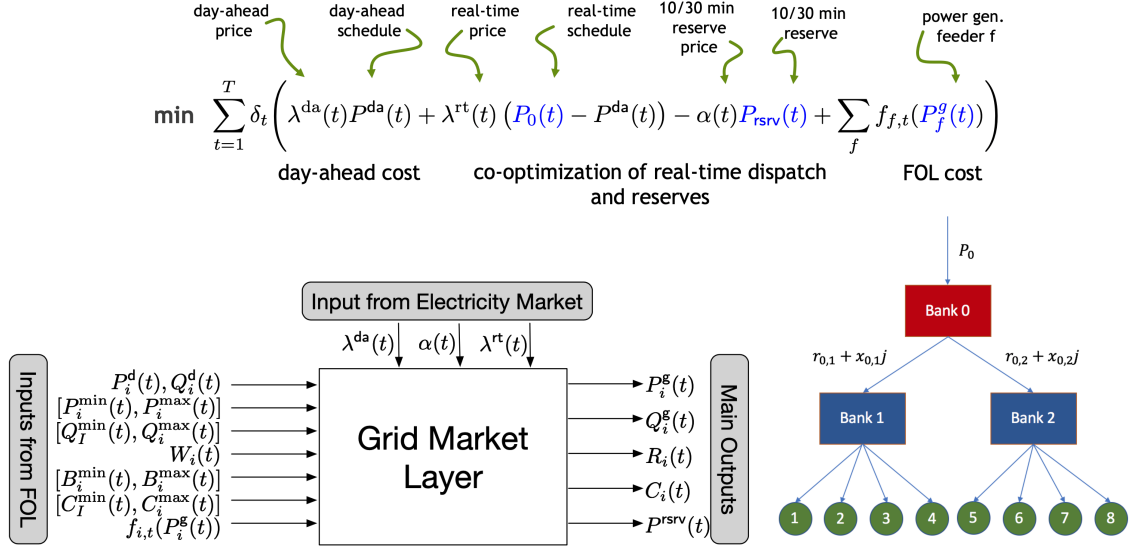
Figure 10: (Top) Deterministic formulation of the GML with day-ahead, real-time, and operating reserve prices representing multi-market participation. (Bottom-left) The inputs and outputs of the optimization module (Bottom-right) Initial rendering of GML's network of feeders was based on the schematic of the O&R Allendale, NJ system comprised of two large transformer banks each supplying four feeders. Bank 0 is connected to the transmission systems. Each transformer bank (banks 1 and 2) has an apparent power capability of 35MVA and base voltage at 69kV. Later in the project, we employed the NYISO subtransmission system for the FOL to incorporate 100s of feeder which are interconnected from a meshed network of transformer banks rather than the initial radial concept.

in the day-ahead forecast. In light of the potential price differences and the chance for arbitrage across stages, the GML may indeed predict *two-stage price differences* and over- or under-procure energy to minimize net cost.

- *Real-Time Market*: The real-time market runs to offset any deviation from the day-ahead schedule for each 5-minute slot before actual operation. This rolling market-clearing implies that the GML has the chance to update its *commitment to procure energy* in the real-time market for the next slot with the latest information, e.g., *real-time price predictions*, after observing the market outcome of the current slot. Indeed, the GML uses a scenario-based approach to predict future prices based on a set $\mathcal{S}$ of dominant scenarios of price changes, i.e., $\Delta\lambda_s^{rt}(\tau), \ \tau = 1, 2, \ldots, T^{pred}, \ s \in \mathcal{S}$, with respect to the latest price realization, where T^{pred} is the length of prediction. For instance, at time t, given the latest real-time price $\lambda^{rt}(t-1)$, the forthcoming prices are predicted as $\lambda_s^{rt}(t-1+\tau) := \lambda^{rt}(t-1) + \Delta\lambda_s^{rt}(\tau), \ \tau = 1, 2, \ldots, T^{pred}, \ s \in \mathcal{S}$. These scenario-based predictions are extracted from NYISO-based real-time prices [49], and Fig. 11a illustrates an example of 3 scenarios of price changes with the prediction length of 2 hours for a particular time of a day.

- *Ancillary Service Market:* We will specifically focus on the ancillary service of 5-min operating reserves from NYISO. The GML, while participating in the real-time market, can simultaneously provide reserve service by tracking designated commands within a committed bound/capacity. Likewise, it can manage and update *reserve commitments*

5 minutes ahead using the latest information, e.g., *reserve price predictions*, due to the repeatedly rolling market operation. The GML obtains the future reserve price predictions $\alpha_s(\tau)$, $\tau = 1, 2, \ldots, T^{pred}$, $s \in \mathcal{S}$, using the same scenario-based approach, except that the scenarios are directly defined on reserve prices rather than price changes. Note that due to the strong coherence between real-time prices and reserve prices, the scenarios $s \in \mathcal{S}$ are clustered jointly based on data from NYISO historical data. Figure 11b shows an example of reserve price scenarios acquired together with those of real-time price changes in Figure 11a.

(a) Real-time price change scenarios

(b) Reserve price scenarios

Figure 11: An example of scenario clustering for real-time price changes and reserve prices.

- *Peak Demand Charge:* We include a GML mode that accounts for peak demand charge, which assigns a large cost to the peak demand occurring during a specified period, e.g., a month. This one-time payment comprised of a unit price way higher than average energy prices, e.g., for a NY utility, the is price $\gamma = \$10,000/\text{MW}$ per month. The GML peak shaving mode allows utilities to use this mode to reduced this significant expenditure.

GML Formulation and Implementation: At the real-time five-minute timescale, we first propose a scenario-based approach to account for the uncertainty in real-time and reserve prices. Consider a finite set of scenarios $\mathcal{S}$ of these price sequences extracted from historical data. For a predetermined sequence range from t_1 to t_f, each scenario $s \in \mathcal{S}$ is given by $s := \{(\pi_s, \lambda_s^{rt}(t), \alpha_s(t)) \mid t \in \{t_1, t_2, \cdots t_f\}\}$, where π_s is the corresponding probability of occurrence with $\sum_{s \in \mathcal{S}} \pi_s = 1$, and $\lambda_s^{rt}(t)$ and $\alpha_s(t)$ are the predicted real-time and reserve prices, respectively.

A receding horizon implementation framework is proposed to compute the optimal feeder dispatch trajectories subject to the GML's AC sub-transmission network with $|N|$ nodes, and $|F|$ feeders. We set a moving prediction window from t_i to $t_i + T - 1$ with all the scenarios in $\mathcal{S}$ accounted for. At each time $t \in \{t_i, \cdots, t_i + T - 1\}$, the following control variables corresponding to scenario $s \in \mathcal{S}$ are considered. On a feeder f, the real and reactive solar generation are denoted as $P_{f,s}^g(t)$ and $Q_{f,s}^g(t)$. The VB energy and power are $B_{f,s}(t), R_{f,s}(t)$. At a node i, the real and reactive nodal injections are denoted as $P_{i,s}(t)$ and $Q_{i,s}(t)$, and the voltage magnitude and phase angle are $v_{i,s}(t)$ and $\theta_{i,s}$, respectively. The total energy and power reserved of the GML are $B_{rsrv,s}(t)$ and $P_{rsrv,s}(t)$. We use U_s to denote all the control

variables in the GML problem, and it is given by

$$U_s(t) := \begin{cases} (P^g_{f,s}(t), Q^g_{f,s}(t), B_{f,s}(t), R_{f,s}(t)), & \forall f \in |\mathcal{F}|, \\ (P_{i,s}(t), Q_{i,s}(t)), & \forall i \in |N|, \\ (v_{i,s}(t), \theta_{i,s}), & \forall i \in |N|, \\ (B_{rsrv,s}(t), P_{rsrv,s}(t)) \end{cases} = \begin{cases} \text{FOL PV power, VB energy/power} \\ \text{GML nodal injections} \\ \text{Voltage magnitude/phase angle} \\ \text{Total energy/power reserves} \end{cases}$$

and the optimization problem to be repeatedly solved is

$$\min \ \gamma \max\{P_{0,s}(t)\} + \sum_{s \in \mathcal{S}} \pi_s \left[\sum_{t=t_i}^{t_i+T-1} \delta_t \Big(\lambda^{\text{rt}}_s(t)(P_{0,s}(t) - P^{\text{da}}(t)) + \lambda^{\text{da}}(t)P^{\text{da}}(t) \Big) \right]$$

$$+ \sum_{s \in \mathcal{S}} \pi_s \left[\sum_{t=t_i}^{t_i+T-1} \delta_t \Big(-\alpha_s(t)P_{rsrv,s}(t) + \sum_f f_{f,t}(P^g_{f,s}(t)) \Big) \right] \tag{10}$$

subject to

      Feeder bounds   (11)

      Bank apparent power constraints   (12)

      Ancillary service constraints   (13)

      Linearized power flow model   (14)

      Scenario coupling constrains: $U_s(t_i) = U(t_i), \forall s \in \mathcal{S}$ (15)

where $P_{0,s}(t)$ is the net demand acquired in the real-time market at time t in scenario s. In particular, the objective (10) is composed of 5 parts. $\gamma \max\{P_{0,s}(t)\}$ represents the peak demand charge. $\lambda^{\text{rt}}_s(t)(P_{0,s}(t) - P^{\text{da}}(t)) + \lambda^{\text{da}}(t)P^{\text{da}}(t)$ represents the total energy expenditure in both day-ahead and real-time markets. The revenue from reserve provision and solar curtailment penalty are accounted for by $\alpha_s(t)P_{rsrv,s}(t)$ and $\sum_f f_{f,t}(P^g_{f,s}(t))$, respectively. The penalty function $f_{f,t}(P^g_f)$ associated with feeder f at time t and is linear, given by

$$f_{f,t}(P^g_f(t)) = \beta_f(P^{\max}_f(t) - P^g_f(t)), \tag{16}$$

where $P^{\max}_f(t) - P^g_f(t)$ measures solar curtailment and the constant coefficient $\beta_f > 0$ represents the unit cost. The curtailment unit cost was determined based on priority and solar curtailment is the last resource to be utilized, so β_f was set to a high value relative to other prices. The constraint (15) enforces that the first-slot decision variables $U(t_i)$ to be implemented immediately are scenario-invariant that couple all scenarios.

Tasks 3.2 and 3.3: Extend GML to stochastic setting and validate at scale

The GML is extended to stochastic formulation by accounting for 1) price signal uncertainty and 2) solar and demand uncertainty (M3.2.2), thereby improving system reliability. The former is accounted for with a set of representative scenarios, clustering with k-means, and the occurrence probabilities of each cluster. The solar PV and demand uncertainty are accounted for with chance constraints via analytical reformulation to cast the uncertainty as

33

a conservative upper bound on solar PV capacity. Solar PV forecast error analysis informs variance on solar PV forecast errors. Finally, a receding-horizon control (RHC) implementation of the GML offers (via feedback) natural robustness to a set of unknown disturbances and enhances reliability. We then show that the offline (with deterministic formulation) outperforms the online (stochastic RHC) implementation, as expected since the online implementation has imperfect predictions and reserves too much energy from reserve price prediction errors. Overall, to compute the optimal robust RHC dispatch for a system of 12 feeders connected across a simple, radial network with 3 transformer banks takes just 25 seconds, which is substantially lower than the upper target of 300 seconds. However, even for a large synthetic system of 1008 feeders across 252 transformer banks (M3.3.3), the robust RHC implementation of GML takes no more than 180-230 seconds depending on market signal complexity. See Fig. 12 for specific times.
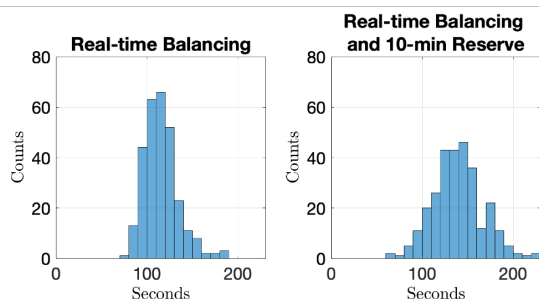

Figure 12: Verifying scalable implementation on the large synthetic radial GML system with 1008 feeders and 252 transformer banks. he maximum solve time for the robust GML is 182 seconds and 231 seconds for real-time balancing and real-time balancing with 10-minute reserves, respectively.

Task 3.4: Develop contingency mode for reliable inter-feeder dispatch and perform benefit analysis

In Year 3, we consulted project advisors in power system economics, Prof. Ben Hobbs from Johns Hopkins University and Prof. Cristoph Weber from University of Duisburg-Essen. We have divided contingencies related to the loss of critical components in either transmission or distribution networks. In addition, the inter- and intra-layer controllers represent another form of contingency modes that are relevant to cyber-components of the grid, including parts of the proposed cyber-infrastructure (e.g., VB dispatch and regulation).

The following two requirements define the priorities of the GML in contingency operation to maintain reliable dispatch: 1) Reserve commitment and end users are of the highest priority, meaning that contingency response needs to ensure that the GML is always able to provide the desired amount of reserve once called upon without shedding any load, thereby improving reliability; and 2) The GML will maintain economic efficiency whenever re-dispatching the feeder operation and interacting with the transmission energy market through the receding horizon control.

In accordance with the reliability requirements identified above, we identify one of the most threatening contingencies to be an outaged or output-constrained feeder, which

abruptly robs the GML of partial solar generation and/or virtual battery capacity. The contingency-secure mode of GML is designed to hedge against the failure to re-dispatch feeders and guarantee the persistent GML operation with the receding horizon control, following the unexpected occurrence of a feeder loss. We adopt the robust technique of $N-1$ contingency constraints to ensure that *even if an arbitrary feeder is lost, the remaining feeders maintain the ability to maintain reliable system operation and live up to the reserve commitments made earlier.*

The contingency-secure mode is formulated below through a minor modification made to the reserve commitment constraints. More specifically, we propose a $N-1$ contingency constraints on the operation of virtual batteries

$$\sum_{f' \neq f} B_{f'}(t) \geq B_{\mathsf{rsrv}}(t), \ \forall f, \tag{17}$$

to replace the original constraint: $\sum_f B_f(t) \geq B_{\mathsf{rsrv}}(t)$, where $B_f(t)$ is the energy on feeder f and $B_{\mathsf{rsrv}}(t)$ is the total energy reserves. The new $N-1$ contingency constraint (17) requires that given any feeder outage, the total virtual battery state-of-charge of the remaining feeders should still be able to provide the maximum possible called reserve $B_{\mathsf{rsrv}}(t)$. In other words, the reserve commitments made earlier will continue to be realizable for contingencies consisting of one feeder loss.

The contingency-secure mode prepares the GML for potential contingencies of an arbitrary feeder outage and enhances its reliability in terms of maintaining participation in both the energy and ancillary service markets. We further propose a practical contingency-recovery mechanism encoded in the receding horizon implementation that immediately responds to the occurrence of a contingency and gradually recovers the GML to the contingency-secure condition by taking over the re-dispatch of feeders in the interim. Such a mechanism provides a holistic contingency solution for GML: first, upon a contingency, the spare energy stored in the virtual batteries due to the conservative enforcement of (17) is released to maintain the capability of fulfilling already-made reserve commitments; second, prompt steps are meanwhile taken to restore the contingency-secure mode such that the GML is ready for any possible follow-up contingencies.

The contingency-secure mode is demonstrated through a one-day GML run with a simulated contingency at time slot 186. Fig. 13(Left) compares the two trajectories of the interface power $P_0(t)$ of the GML with the transmission network market under the contingency-secure mode with and without this contingency. More explicitly, the difference between the two trajectories (w minus w/o) is also plotted therein. The subtle difference suggests that the contingency-secure mode stores enough backup energy in the virtual batteries to accommodate a contingency without propagating the effect outwards to the transmission network. Fig. 13(Right) more explicitly demonstrates the operating principle of the contingency-secure mode through the evolution of the difference between the aggregate state-of-charge B_{total} and the worst-case $N-1$ state-of-charge[3] $B_{total} - max\{B_f\}$. Even without a contingency, the

---

[3]By worst case, we mean the aggregate state-of-charge by excluding the feeder with the most virtual battery energy.

difference, i.e., the extra amount of virtual battery energy, is put aside conservatively. Once a contingency occurs, starting from time slot 186 (15:25-15:30), this backup energy is released to hedge against the loss of storage capability, which is reflected by the sudden drop of the difference. After the recovery period, the difference rises and restores to its normal value.
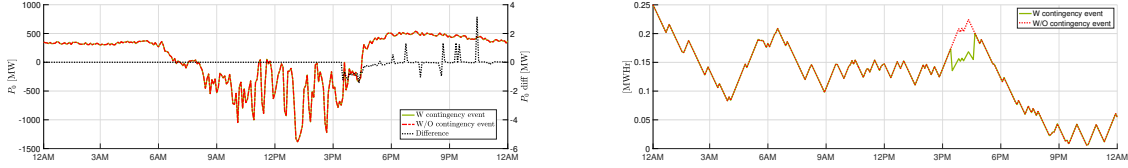

Figure 13: *(Left)* Contingency-secure mode: comparison of the net power procurement $P_0(t)$ in a day with and without a contingency. *(Right)* Comparison of contingency and non-contingency runs of contingency-secure mode: difference between aggregate SoC B_{total} and worst-case $N-1$ SoC $B_{total} - max\{B_f\}$.

Task 3.5: Formalize and quantify tradeoffs between short/long-term flexibility and market-participation

Illustration of GML benefit analysis

To compensate for the accuracy loss of the linearized power flows, we introduce the following three-layer tuning mechanism, as depicted in Figure 14. The first and third layers are both power flow layers, which resort to commercial power flow solvers, such as PowerModels.jl [50]. In our first layer, we assume that the demand is given as estimated, the solar generation is provided at its estimate maximum, and the virtual storage remains idle. We then attain the power flow setpoints $(P_i^*, Q_i^*, V_i^*, \theta_i^*)$ for $\forall i \in \mathcal{N}$ with PowerModels.jl, which are passed to the second layer, the approximate GML model layer. The approximate GML model layer solves for the optimal feeder-level solar and VB scheduling. Note that the resulting power flows are at best approximate, and need to be tuned in the third power flow layer. Through the third layer, accurate power flow is guaranteed based on the solution from PowerModels.jl, given the feeder-level scheduling determined from the second layer. We now provide a set of numerical results of a sub-network of New York Independent System Operator (NYISO). The solar generation and demand profiles are obtained from the utility for a day in August 2016. We adopt the price trajectory of August 2019, and consider the following three scenarios in our illustration:

- *Scenario #1:* This *baseline* scenario assumes that no VB is available, i.e., $B_f^{max}(t) = 0$, $\forall f, t$, and that all solar runs at full capacity, i.e., $P_f^g(t) = P_f^{max}(t)$, $\forall t$, for both the day-ahead and real-time markets.

- *Scenario #2:* In this *GML* scenario, the GML has the ability to curtail the solar usage and charge/discharge the VB.

- *Scenario #3:* In this *GML+peak-shaving* scenario, the peak-shaving mode is implemented, and the unit price for peak demand charge is set to be $\gamma = 10,000$ \$/MW.
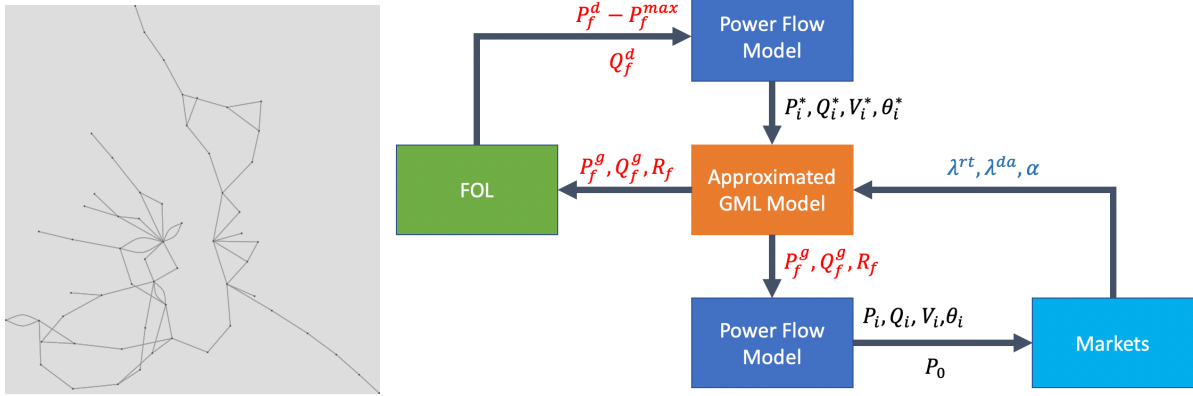
36

Figure 14: (Left) Due to the meshed nature of ORU's subtransmission network that interconnects the transformer banks and feeders, the GML must be enhanced with a novel three-layer tuning system. (Right) The approximate GML model layer solves for the optimal feeder-level solar and VB scheduling. Note that the resulting power flows are at best approximate, and need to be tuned in the third power flow layer. Through the third layer, accurate power flow is guaranteed based on the solution from PowerModels.jl, given the feeder-level scheduling determined from the second layer.

Table 2: Economic benefits of GML.

	Without VB	VB: 75 MW+187.5 MWh		VB: 150 MW+375 MWh	
Scenario	*#1*	*#2*	*#3*	*#2*	*#3*
Real-time cost ($)	428 330	425 981	426 053	**424 322**	424 486
Solar curtailment cost ($)	0	0	0	0	0
Peak cost ($)	12 609 000	13 299 920	12 150 240	14 061 360	**11 881 330**
Total cost ($)	13 037 330	13 725 901	12 576 293	14 485 682	**12 305 816**

In Scenarios #2 and #3, we evaluate the economic impact of the VB size. Two sets of VBs are tested: 1) aggregated energy capacity 187.5 MWh and power rating (maximum charging or discharging rate) 75MW; 2) aggregated energy capacity 375 MWh and power rating 150 MW. The detailed cost comparison is summarized in Table 2. In particular, the day-ahead and real-time costs are both calculated based on net procurement from the transmission-level markets, i.e., $\sum_{t=1}^{T} \lambda^{\mathrm{da}}(t) P_0^{\mathrm{da}}(t) \delta_t^{\mathrm{da}}$ and $\sum_{t=1}^{T} \lambda^{\mathrm{rt}}(t)(P_0 - P_0^{\mathrm{da}}(t))(t)\delta_t$. The solar curtailment cost is adopted from (16), and the peak demand charge is explicitly $\gamma \cdot \max_t \{P_0(t)\}$.

As we expect, the baseline scenario incurs the highest real-time cost. Given the same VB specifications, the GML scenario reduces the real-time cost most, however creates the highest peak as a result. The lowest cost and lowest peak is guaranteed in Scenario #3. Besides, our results conforms with the intuition that a larger VB leads more savings. Figures 15 and 16 depict the net procurement from the transmission market and the VBs' aggregate behavior, respectively, for test with VB aggregated energy capacity 375 MWh and power rating 150 MW. We can observe that in Scenario #2, the VB is more active between 17:00 to 20:00, trying to arbitrage across the two-stage markets. However, in Scenario #3, the peak-shaving mode always minimizes the peak net procurement, which flattens the net demand curve.
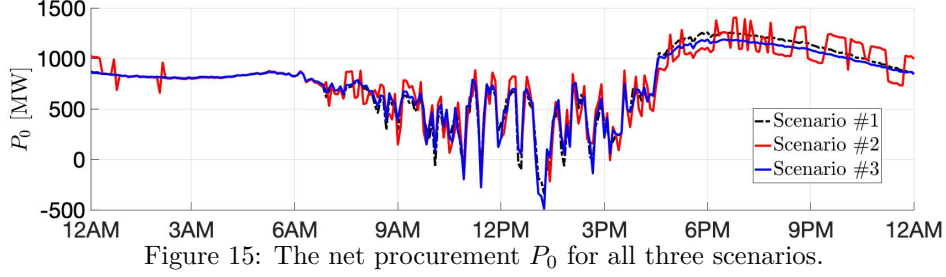
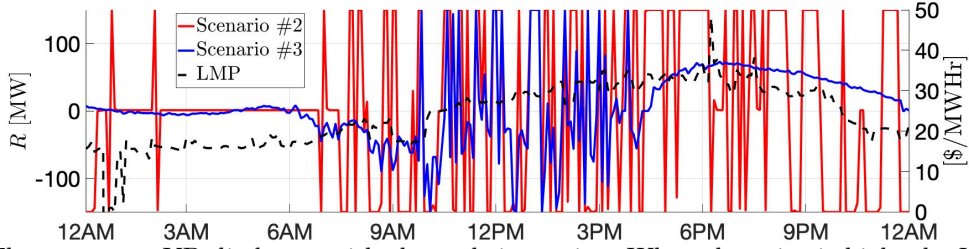Figure 15: The net procurement P_0 for all three scenarios.

Figure 16: The aggregate VB discharge with the real-time price. When the price is high, the VB tends to discharge to avoid a high real-time cost, e.g., 6:15 PM.

We further investigate the economic efficiency of these two sets of VBs. The economic efficiency is quantified by the per-unit savings for VB energy capacity with respect to the baseline-scenario cost. These results are listed in Table 3, which show that although larger VBs yield more savings, the marginal benefits of VB capacity and power rating decrease. Interestingly, it can be shown that at $6120/$MW$ peak savings for the 75MW/187.5MWh VB Scenario #3, the GML achieves an economic efficiency of 61% given the peak price of $10,000/MW. The loss of efficiency from 100% is a function of the (conservative) nature of the stochastic GML along with the FOL's feeder limits on headnode flexibility.
Milestones delivered:

- M (ST-3.2.1) Implementation and validation of the model with a small test grid that can be verified analytically (3 FOLs and two timescales).
- M (ST-3.2.2) Solve the decomposition problem for small-scale feeder (50-100 nodes per feeder, three-phase unbalanced) test cases with >10 FOL elements to within standard solver tolerances.
- M (ST-3.3.3) Solve time for stochastic GML decomposition problem for large-scale test network developed in subtask 4.1.4 with a focus on coordinating and dispatching > 1000 FOL elements.
- M (ST-3.4.2) Resilient GML operation for a large realistic test case: during a period following a "reasonable" contingency, feeders under GML can compute necessary re-dispatch signals to reset

Table 3: Per-unit savings for VB capacity and power rating.

	VB: 75 MW+187.5 MWh		VB: 150 MW+375 MWh	
Scenario	*#2*	*#3*	*#2*	*#3*
Real-time saving	**12.59 \$/MWh**	\	10.72 \$/MWh	\
Peak saving	\	**2448.80 \$/MWh**	\	1941.49 \$/MWh

38

aggregate interaction with markets while operating within grid limits.

Task 4: Technology Demonstration

The goal of Task 4 is to demonstrate scalability, practicality, reliability and commercial viability for a DSO in Year 2030. To achieve this goal, Year 1 focused on data procurement, processing (e.g., network reduction), and visualization with iPGA and for each layer (GML, FOL, STL) to complete stand-alone proof of concept validation. In Year 2, we focused on small deterministic test systems using the reduced networks from Year 1. Year 3 would then complete validation and demonstration at scale and incorporate stochastic uncertainties associated with demand and solar PV forecast errors.

Task 4.1 - Data gathering and processing

In the first year, the goal on data gathering and processing was to procure large networks, SCADA data from utility partner ORU, and representative solar PV of NY state. ORU was a fantastic partner in the process and provided necessary data and lent their time to the project to allow us to properly understand the networks. In the end, we processed 3 large feeders from ORU's substations in UVM's software tool iPGA. One feeder and its reduction is shown in Fig, 17, which is served from a substation with a 35MVA transformer. The full network has about 1200 primary nodes (at 13.2 kV) and about 450 secondary nodes (at 240/120 V) of which are multiple service points. In addition to network/equipment parameters, ORU provided hourly SCADA measurements at the head-node (kW, kVAR, power factor, Amperes) and off/on-peak nodal disaggregation factors for primary node loads. Secondary loss parameters were filled in based on a common loss factor that minimized the error between AC load flow data in SCADA and simulated load flow results from GridLab-D. We placed PV arrays at service points in 1:1 proportion to the nodal peak loads and rounded to the nearest 5 kWdc system value, resulting in 3.2 MW installed capacity in the feeder (the peak demand is 3.3 MW). We power these panels using historical (2017) minutely irradiance data provided by IAB member (CPR).

Task 4.2 - Small-scale Software and Hardware Validation

- At the end of Year 2, we conducted the small-scale, coupled software simulation of the GML-FOL-STL-DSSE setup (M4.2.2), we sent the UVM students to PNNL for the summer 2019 where they worked closely with their PNNL counterparts to implement the FOL/DSSE and STL schemes and set up testing. This was quite effective use of resources and resulted in successfully exceeding performance in terms of targets. Specifically, we showed that 1) the GML's set-points could be tracked accurately by the FOL; 2) computation times were all below 30 seconds; 3) FOL was executed every minute; 4) STL DERs track their VB set-points; and 5) DSSE is able to correctly estimate voltages more than 99.85% of the time. However, this was the small test-case of just 101 nodes in the reduced network.
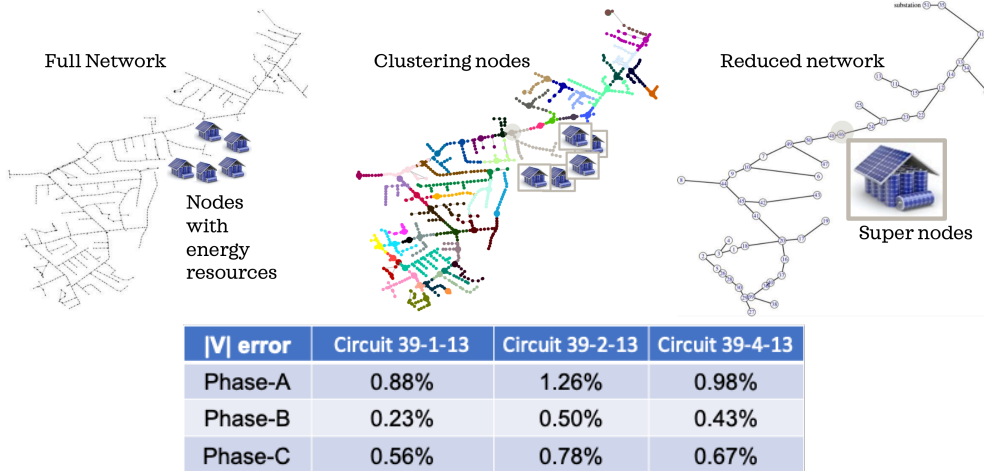
Figure 17: (Top) Network reduction process implemented in iPGA (left-to-right) for one of three full networks supplied by utility partner ORU. iPGA first partitions the full network of 1200 primary nodes into 50 clusters based on electrical and physical proximity and chooses super nodes from each cluster. The super nodes then identity the buses for which Kron Reduction is applied in the three-phase network to create a $50 + 1 = 51$-node reduced network. All demand and VBs within the super node's cluster are aggregated linearly to that super-node to complete the network reduction process. Note that a $130 + 1 = 131$ node reduced version of the network was also created. When you add in the super loads, the networks double in size from 51 to 101 and 131 to 261 (since there are no loads at the head-node). (Bottom) The table of maximum absolute percent error (Max-APE) in intra-cluster voltage magnitudes compares how representative the super node voltages in the reduced network are of the cluster's voltages under AC load flow analysis. It is shown that the Max-APE is much smaller than the milestones' required 2% RMSE.

- Separate from the software simulation, in M4.2.2., we wanted to conduct a hardware-in-the-loop (HiL) simulation. However, owing to the scale of the system, real hardware was not possible to interface. Instead, we considered emulated devices that communicated in real-time over a communication simulator of IEC protocols to represent a realistic DSO communication system. That is, together with collaborators at NIST, we showed with OPAL-RT and a network simulator for IEC protocols that the presented framework for managing DERs was technically implementable in terms of communication requirements of an STL and the real-time intra- and inter-feeder control.

Validating proof of concept: Communications between FOL-STL layers (M4.2.2): Validating the latency, throughput, and data scalability challenges associated with information exchange between FOL, STL, and individual DERs is fairly challenging and best approached via high fidelity simulation on a real-time digital simulator. Noting that these network performance metrics are sensitive to the choice of communication protocol, data exchange formats, and information models; a simulation of intra-feeder control was supplemented with a 'real' implementation of the full stack of IEC 61850 communication protocols.

This method of evaluation was used to assess the real-time feasibility of intra-feeder and STL control communications noting the particularly demanding 1 second loop time of the STL controller. The simulation consisted of a single FOL element represented as a radial distribution feeder with 60 connected DER assets distributed across 15 secondary distribution
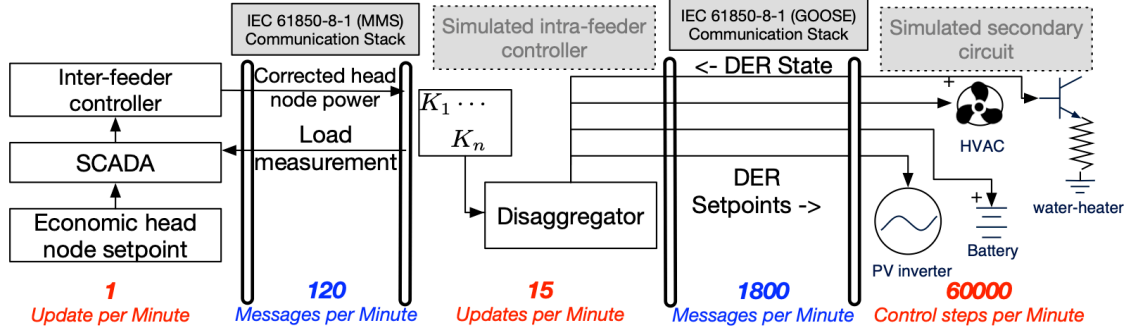
Figure 18: A schematic diagram showing the interacting elements in the validation environment. Here a single feeder and service transformer unit are considered. 60 DER assets are coordinated by the system using IEC 61850 compliant information models and communication protocols.

circuits. Each secondary distribution circuit featured a service transformer augmented with the communication interfaces and hosted between 3 and 5 DER assets. The modeled DER assets were a mix of PV generators and dispatchable loads in the form of electric water heaters and AC units. The entire 60 DER simulation was executed on an Opal-RT OP5600 real-time simulator with 1 millisecond simulation time steps. The temporal scaling between the different computation elements ranges from a 10 ms control loop time for individual DERs, 4 second loop times for the intra-feeder controller, and a FOL update every one minute. All these computational updates are locked to the same hardware clock, ensuring they are coherent with each other.

To interface the simulated components with a real implementation of the communication stack, each DER asset and each service transformer was modeled as an IEC 61850-7-420 logical node [51], receiving individual power setpoints and configuration settings from the DER dispatch algorithm in the intra-feeder controller. These measurements and commands were modeled as IEC 61850-7-2 data objects, exchanged as IEC 61850-8-1 generic, object-oriented substation events (GOOSE) [52]. The full model, including dynamic representations of the DER assets and the IEC 61850 components, was constructed using the Simscape Electrical library and connected to software drivers for IEC 61850-8-1 communication.

An overview of the validation setup is shown in Figure 18. 45 DERs receive ON/OFF commands as IEC 61850-8-1 compliant *DRCC/DERStr* and *DRCC/DERStop* events. The 15 remaining DERs (assumed to be dispatchable PV generators) are provided power curtailment requests as *DRCC/WSet* events. 1800 IEC 61850-8-1 GOOSE messages per minute are generated to meet the DER control loop time. The intra-feeder controller in turn interacts with the inter-feeder controller and the FOL using IEC 61850-8-1 Manufacturing Message Specification (MMS) messages (at rate of 120 headnode setpoints received per minute).

The validation aspect of this exercise was to establish whether potential congestion from rapid, periodic updates would adversely affect the performance of the control system at the STL. All IEC 61850 messages produced by the simulation were routed through a data pipeline complete with network routers and data processing buffers designed so that the pipeline would introduce realistic communication delays and errors.

Figure 19 shows the throughput of the data pipeline while performing this experiment.
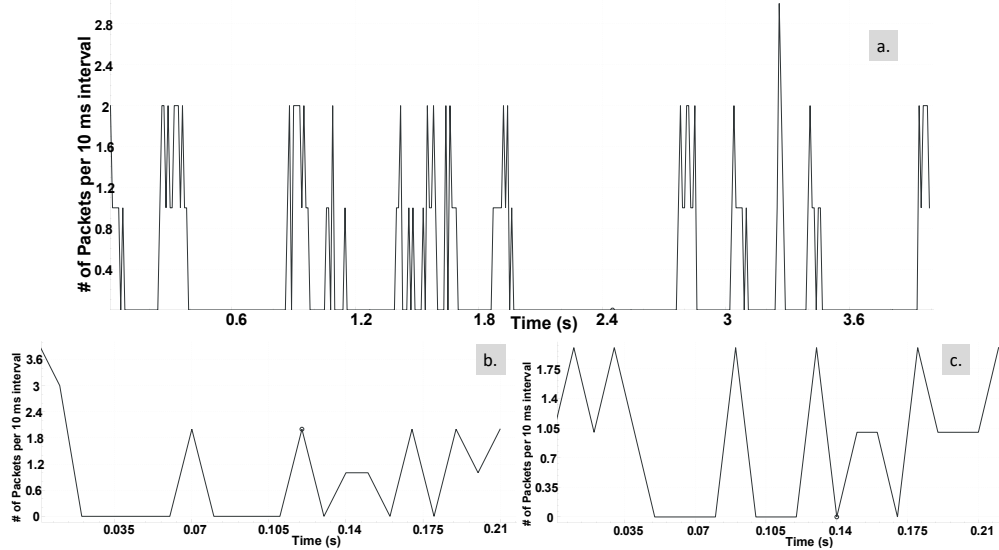
Figure 19: Communication throughput: a. GOOSE exchanges between STL and DERs (average latency ≈ 5 ms) b. Load request correction from FOL to STL (average latency ≈ 10 ms) c. Load estimate query from STL to FOL.

Figure 19(a) shows a histogram of packet arrival rate. The x-axis on the plot shows the total time taken for all 60 DERs to transmit their state and receive commands from the STL. In this particular instance, all 60 DERs were updated in under the update loop time for the STL of 4 seconds. The average latency of the updates was 5.2 ms which is well below the requirement of 100-500ms for intra-feeder controller. Similarly, Figure 19(b) and Figure 19(c) show the stable throughput exceeding the update constraints of the FOL with bounded message latency of approximately 10 ms. Of course, as the number of DERs scale, so does latency; however, since the GML-FOL-STL mirrors the voltage hierarchy of the network, the scale of DERs is contained within each layer. Thus, the promising proof of concept validation presented indicates that the whole scheme is likely to be implementable in practice within a DSO. One key element is needed: smart loads must become open to standards so that we can communicate with them. For PV inverters, this is possible due to SunSpec's set of standards.

Task 4.3 - Large-scale software and hardware demonstration

In the final year, we conducted the large-scale, stochastic simulation that combined GML-FOL-STL-DER together with all three large-scale feeders, connected via NYISO's sub-transmission network of substation transformer banks, and fully realized STLs in each feeeder populated with individually emulated DERs.

Simulation Setup:

- The simulation demonstrates the efficacy of the proposed framework on a subnetwork of NYISO consisting of 150-300 feeders (please see, Fig. 14(left)). Three of the feeders in

42

the NYISO network are fully modeled circuits in Gridlab-D. The three feeders contain 125, 90 and 60 super nodes representing an aggregation of 1213, 936 and 594 STL nodes respectively. The VBs models for the loads are incorporated into the GridLab-D model.

- Given the VB parameters, a subset of the STL nodes (representing a super node in the reduced model) in each of the feeder are populated with air-conditioners and electric water heater representing the available flexibility based on the generated virtual battery parameters. The other super-nodes are augmented a Gridlab-D battery object with capacity and power rating identifical to the corresponding virtual battery.

- Each of the super nodes is also augmented with solar PV inverters to reach 50% of demand (by annual energy). The inverters were sized appropriately to ensure enough reactive power flexibility. The Kron-reduced feeder along with the newly created batteries and inverters formed the final GridLab-D model used in the simulations[4].

- The project's novel framework required integration and complex interactions between the FOL, GML and STL algorithms and the GridLab-D model, which simulated the feeders and individual DERs in each feeder's STL elements. We used Framework for Network Co-Simulations (FNCS), open-source co-/multi-simulation framework which uses a federated approach for integrating multiple simulators, for co-/multi-simulations of the aforementioned software. Exchange of information, including synchronization of simulator clocks among power and market simulators is maintained using central agent called FNCS broker. Since FNCS has the capability of co-/multi-simulations of multi-domain simulators, it provides an efficient solution to synchronize the different algorithms with the Gridlab-D model. Also, FNCS can synchronize multiple packages, tools, and simulators hosted in different machines, which ultimately ensure modular and parallel development and integration of different packages.

  FNCS receives information from the GridLab-D model such as the battery state of charge needed for the FOL algorithm. The information is exchanged in the form of key-value pairs which then have to be parsed before being communicated to the algorithms. This is done using a Python API which parses the data received from FNCS before sending them to a Julia server that contains the GML, FOL and STL algorithms.

  Once the Julia server receives the data from Python, DSSE uses the voltage measurements to compute the state of the system. The FOL algorithm uses the battery state of charge values and the GML tracking signal to compute the new active and reactive power set-points of the inverters. These values are returned back to the Python API which then converts it into key-value pairs before passing it back to FNCS. FNCS then relays this information to GridLab-D which updates the inverter set-points, thereby completing the loop. In the following subsection, we will present detailed results for the three fully-modelled feeders for two different scenarios.

---

[4]Note that under an unexpected topology change that preserves the radial nature of the feeder, the reduced network should be able to faithfully represent the corresponding network with an appropriate net-demand reduction (from an outaged lateral) or an effective outage in the reduced network outage.
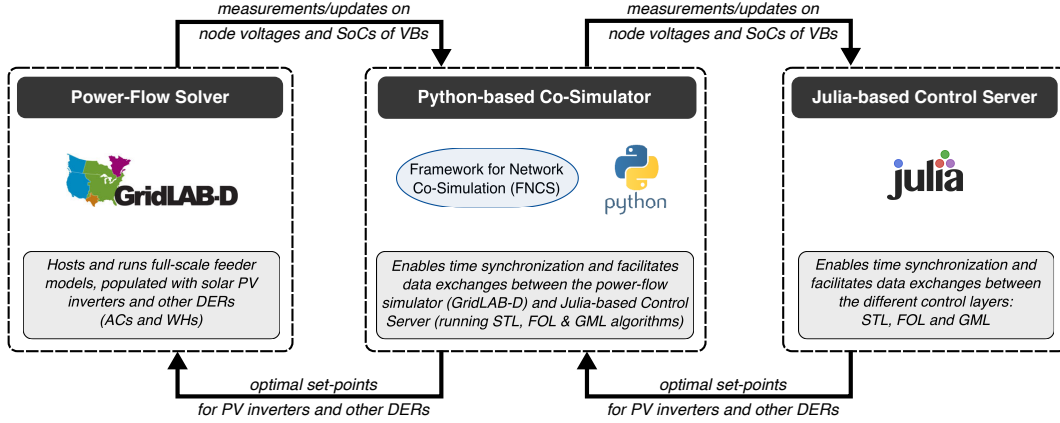
Figure 20: The integrated co-simulation environment for numerical validation of the coupled hierarchical stochastic control algorithms (STL, FOL and GML) with large-scale simulations of distribution feeder models populated with solar PV and other DERs.

- The simulation was conducted for one of the peak hours (Aug 01st 11:00 AM - 12:00 AM). The two scenarios were completed: *peak shaving* and *cloud cover*. We will showcase peak-shaving.

Consider the peak-shaving scenario with and without VBs. Then, the GML can produce an economically optimal trajectory for every feeder, such as seen in Fig. 21, which starts from 11:00am. Next, Fig. 22 shows the system-wide tracking performance of three fully-modeled feeders, which is excellent. Then, Fig. 23 depicts a comparison of voltage profiles with and without VBs to highlight reliability benefits from FOL's optimization of STL's controllable PV and VB resources. In Fig. 24, we can see that the VBs' energy constraints are satisfied during the period of tracking in the peak-demand hour (i.e., comfort requirements are met). Importantly, VBs do not just improve voltage profiles, but also aid in reducing any solar PV curtailment during the tracking period as shown in Fig. 25. For example, in Feeder 3, at 11:10-11:16, VBs prevent a 2MW curtailment event. Finally, Table 4 records the salient tracking and voltage profile metrics of the simulation.
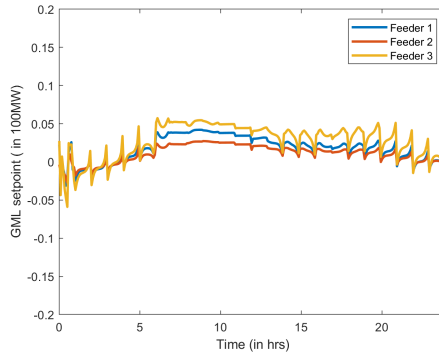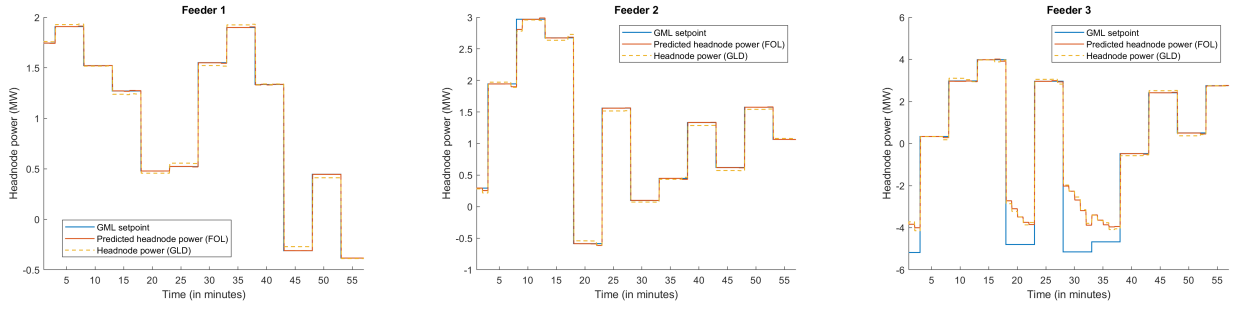

Figure 21: The 24-hour GML real power setpoint for the fully modelled feeders starting from 11:00 AM
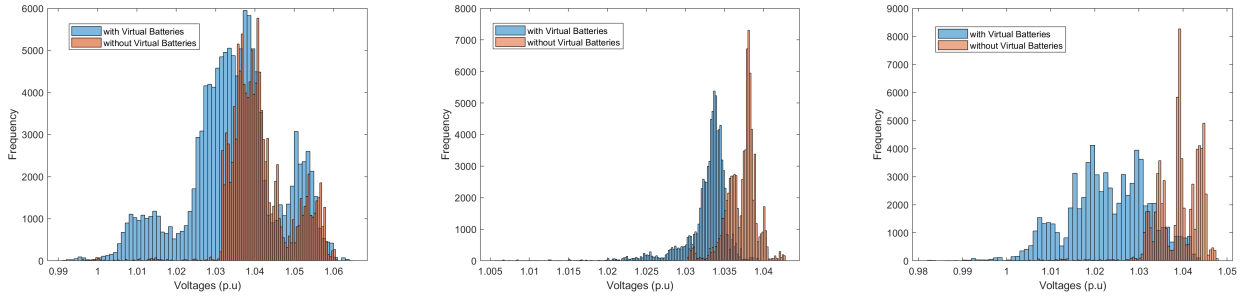
(a) Feeder 1   (b) Feeder 2   (c) Feeder 3

Figure 22: GML setpoint tracking performance for the fully modelled feeders. Note that Feeder 3 experiences a larger-than-expected forecast error that leads the GML to push the feeder beyond its export limits and the FOL sacrifices tracking to ensure reliability (as designed).
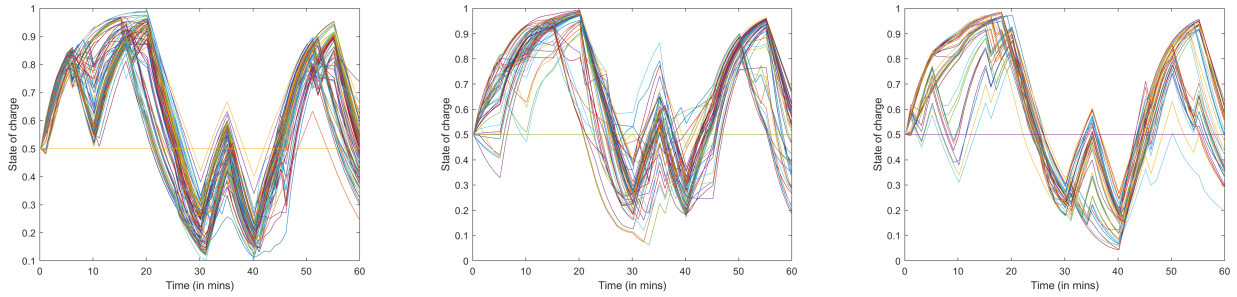

(a) Feeder 1   (b) Feeder 2   (c) Feeder 3

Figure 23: Voltage distribution for all nodes from 11:00 AM to 12:00 AM. Clearly, VBs aid in regulating and improving the feeders' voltage profiles.

(a) Feeder 1   (b) Feeder 2   (c) Feeder 3

Figure 24: Evolution of state of charge (SoC) for VBs in each feeder.

Table 4: Tracking RMSE error and upper 95th percentile of the nodal voltage distribution when virtual batteries are utilized

	RMSE	Voltage with VB	Voltage without VB
Feeder 1	14 kW	1.053 p.u	1.058 p.u
Feeder 2	20 kW	1.035 p.u	1.041 p.u
Feeder 3	90 kW	1.038 p.u	1.047 p.u

<div style="text-align:center">(a) Feeder 1   (b) Feeder 2   (c) Feeder 3</div>
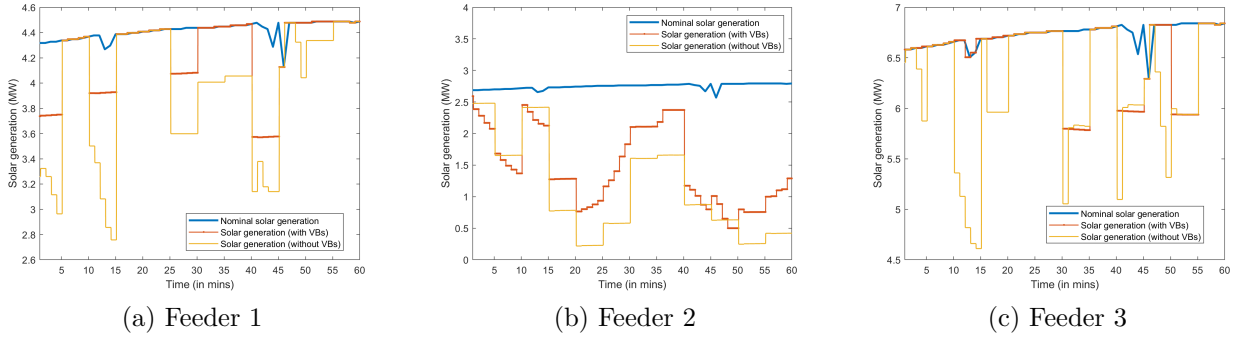
Figure 25: Total PV output for all super nodes from 11:00 AM to 12:00 AM in each feeder.

Finally, we we illustrate the performance of both the intra-feeder and inter-feeder control systems via simulation.

Proof of Concept validation: Inter-layer real-time feedback control

- Since the specific network is not important in this setting, consider a simplified GML that provides economic set-points to two simplified feeders that are based a modified IEEE 37-node single-phase equivalent circuits and a simplified FOL with batteries representing the VBs. Three sets of DERs, specifically containing 28, 28, and 26 water heaters, are assumed to be present in each feeder at different locations (specifically, where the base demand is 140 kW, 140 kW, and 126 kW respectively, to match the total rated power of the devices) making a total of 164 water heaters, each of rated power 4.5 kW. Under these simplified conditions, Fig. 26(Left) shows the results of a 3-min simulation to illustrate the effectiveness of inter-layer feedback control in rejecting disturbances while tracking the GML economic reference (shown as a yellow dashed line). We showcase three examples of disturbance classes that can be mitigated using the intra-feeder and inter-feeder controllers. First, at around 8 s, a step disturbance (e.g., due to persistent cloud cover) is added to some nodes of both the feeders. Since the change in total head node power is less than the dead-zone limit of the inter-feeder controller (assumed to be 72.7 kW, which is 10% of the total base demand in one feeder), only the intra-feeder controller remains active. The intra-feeder controller, combined with the optimization-based device-level dispatch, updates once every second and improves the tracking of the economic reference compared to the case where there is no real-time control (purple dash-dotted line). Second, at around 35 s, random noise is added (e.g., due to intermittent cloud cover). It can be seen that with real-time control, the variance of the total head node power is reduced. Finally, at around 88 s, 2 sets of DERs in the second feeder are assumed to be unexpectedly set to 'zero' power perhaps via malicious cyber intrusion. Since this is a major contingency, and the power change is more than 72.7 kW, the inter-feeder controller becomes active. Acting with a loop delay of 5 seconds, it brings the total head node power close to the desired value using remaining active devices from both feeders using the optimization-based dispatch. Thus, the real-time control mechanism is demonstrated as effective in mitigating various classes of disturbances. Moreover, the computation of the real-time control action, including the optimization-based device-level
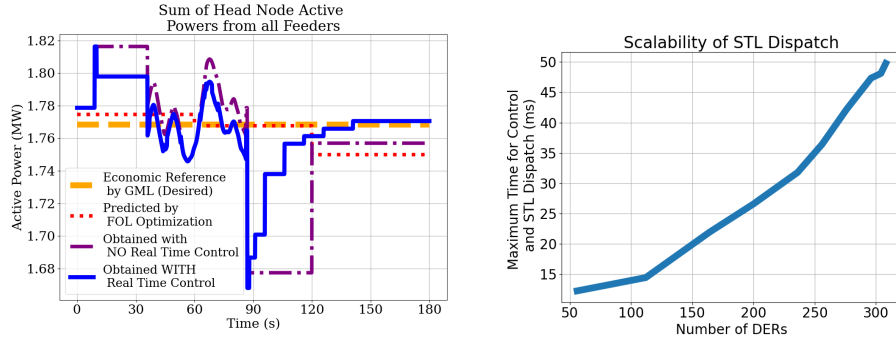
Figure 26: (Left) Simulation of intra- and inter-feeder controllers correcting static set-points to improve tracking. (Right) Scalability of real-time control and STL Dispatch.

dispatch, took a maximum of 23 ms per control action in the simulation. Computational delays seem to be significantly shorter than the expected control action every 1 s or 5 s. Also, Fig. 26(Right) shows the time required for control and dispatch of STL elements when the number of DERs/STL elements increases. It can be seen that even for 300 devices, the real-time STL control and dispatch takes less than 50 ms. We expect that the proposed controller is real-time feasible at scale.

Milestones delivered

- M (ST-4.1.4) Statistically equivalent network reduction: nodal/branch-reduction in networks from data will cause small voltage/current deviations with respect to full three-phase network simulations for all time-steps for a month in summer and a month in winter.

- M (ST-4.2.1) Demonstrate satisfaction of all relevant technical targets by deterministic simulation of coupled DSSE+FOL+GML from the small-scale system developed and created in Sub-task 4.1.4 (>50 nodes per FOL element; >10 FOL elements in the GML for more than >1000 DERs modeled as virtual batteries).

- M (ST-4.2.2) Demonstrate satisfaction of all relevant technical targets by deterministic HiL simulation of coupled DSSE+FOL+GML from the small-scale system developed and created in Sub-task 4.1.4 (>50 nodes per FOL element; >10 FOL elements in the GML for more than >1000 DERs modeled as virtual batteries [VB]). At least one VB is based on at least 10-20 physical hardware devices that emulate individual DERs. Separately, the real-time STL element controller response of a single VB is validated with HIL simulations.

- M (ST-4.3.2) Coupled DSSE+STL+FOL+GML with GridLab-D or Open-DSS for large-scale Realistic ORU system developed in Subtask 4.3.1 over representative days for a one-year period in the year 2030 in the Northeastern United States

- M (ST-4.3.3) The > 100 real-time, cyber-enabled, emulated DERs are split into a couple STL elements (10-20 DERs/element) within 1-2 FOL elements, which is then subject to virtual STL and FOL entities.

Significant Accomplishments and Conclusions

The program was highly successful in all regards and successfully achieved all major milestones, final deliverables, and technical objectives over the course of the project.
A brief description of particularly noteworthy accomplishments are presented:
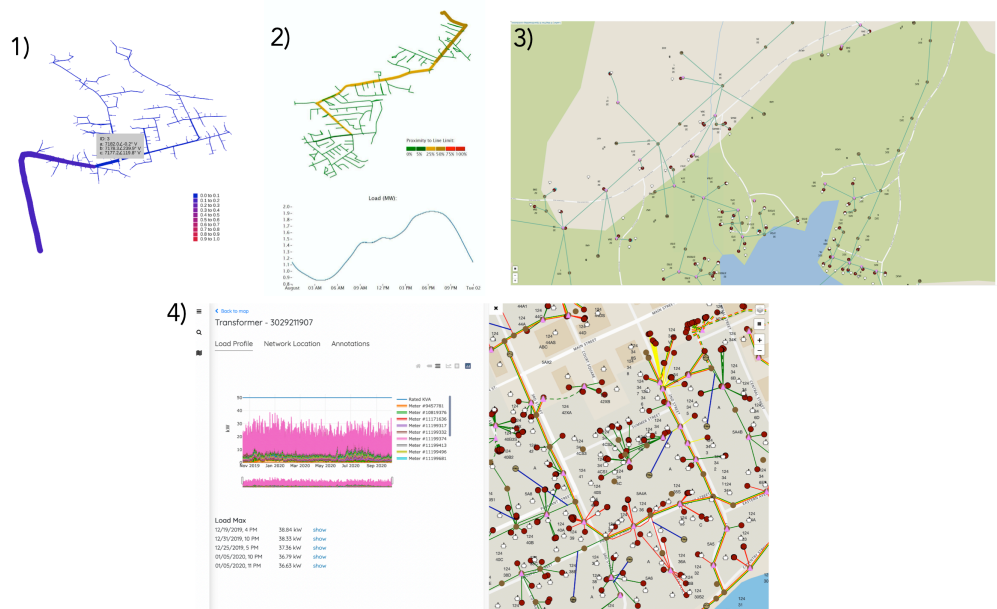
47

Figure 27: The evolution of the interactive distribution grid analytics (iDGA) tool from pre-project is in 1) to end of project's Year 2 in 2) to licensee Packetized Energy 3) who have advanced the tool to integrate AMI, network, geographical data, and SCADA data in 4).

- The GML has been developed to effectively and reliably incorporate optimization of temporally coupled energy resources across meshed subtransmission systems and wholesale energy market services across multiple timescales.

- The FOL's stochastic, multi-period, AC OPF formulation handles different grid assets, integrates DSEE and network reduction techniques and represents an excellent contribution to the power systems community. In addition, it has potentially a lot of value, if we can get the idea adopted in the near term.

- The flexibility of a group of heterogeneous DERs has been characterized with a novel advanced methodology based on ML and the STL DER control method is highly scalable. This is a huge achievement.

- UVM's iPGA has been licensed and is in use by utilities in the US. Please consider the evolution of iPGA in Fig. 27. Specifically, we adapted iPGA for ORU's network and SCADA data, which were in EDD's DEW format. In this project, we then added the ability of iPGA to solve and visualize minutely load flows of ORU's network to allow a user to select the time of interest and show network power flows along with 3-phase voltage and current values. Packetized Energy has since licensed the software and added a GIS engine and front-end that integrates AMI and SCADA data, including network switches and substations, to provide a more user-friendly *GridSolver* tool for distribution system planning and operations engineers.

- The Intra-feeder and Inter-feeder controllers represent a clear, reliable and practically implementable approach to integrate control within a DSO.

- The team has submitted over 30 papers and given numerous talks at universities and

industry with one publication from the entire team and summarizing key project outcomes (see [36]).

The project outcome is a novel hierarchical DER coordination scheme that through large-scale simulations and real-time validation is shown to be technically scalable, reliable and practically implementable within a utility setting. Specifically, simulation results illustrate how coordination of DERs improves both system reliability and economics and enables a greater penetration of solar PV in distribution feeders.

Inventions, Patents, Publications, and Other Results

Awards

1. Enrique Mallada, MINDS Research award, JHU Office Of VP of Research 2019
2. Enrique Mallada, NSF CAREER Award, National Science Foundation (ECCS) March, 2018
3. Dennice Gayme, Simons Fellowship, Isaac Newton Inst. For Mathematical Sciences Q1, 2019
4. Enrique Mallada, Dennice Gayme, Discovery Award JHU, April, 2019
5. Mads Almassalkhi Hall of Fame award, UVM Innovations, April, 2019

Patents/Patent applications

1. P. Racherla, P. Hines, and M. Almassalkhi, *Interactive Power Grid Analytics (iPGA)*, 2020.

Publications (by performance team)

1. (Submitted) S. Brahma, and H. Ossareh, Analysis of Accuracy and Numerical Properties of Stochastic Linearization, SIAM Journal on Numerical Analysis, 2020.
2. (Submitted) Y. Jiang, E. Cohn, P. Vorobev, and E. Mallada, Storage-based frequency shaping control, IEEE Transactions on Power Systems, 2020.
3. (Submitted) N. Nazir and M. Almassalkhi, Grid-aware aggregation and realtime disaggregation of distributed energy resources in radial networks, IEEE Trans. on Power Systems, 2020.
4. (Under review; Rev01) L. S. P. Lawrence, J. W. Simpson-Porco, and E. Mallada, The optimal steady-state control problem, IEEE Trans. on Automatic Control.
5. (Under review; Rev01) Y. Jiang and R. Pates and E. Mallada, Dynamic Droop Control in Low-inertia Power Systems IEEE Trans. on Automatic Control.
6. (Under review; Rev02) N. Nazir, and M. Almassalkhi, Voltage positioning using co-optimization of controllable grid assets in radial networks, IEEE Trans. on Power Systems.
7. M. Almassalkhi, S. Brahma, N. Nazir, H. Ossareh, P. Racherla, S. Kundu, S. P. Nandanoori, T. Ramachandram, A. Singhal, D. Gayme, C. Ji, E. Mallada, Y. Shen, P. You, and D. Anand, Hierarchical, Grid-Aware, and Economically Optimal Coordination of Distributed Energy Resources in Realistic Distribution Systems, Energies special issue on *Building-to-Grid Integration through Intelligent Optimization and Control*, (Accepted) 2020.
8. S. Brahma, N. Nazir, H. Ossareh, and M. Almassalkhi, Optimal and resilient coordination of virtual batteries in distribution feeders, IEEE Trans. on Power Systems, (Accepted) 2020.
9. N. Nazir, P. Racherla, and M. Almassalkhi, Optimal multi-period dispatch of distributed energy resources in unbalanced distribution feeders, IEEE Trans. on Power Systems, 2020.
10. F. Paganini and E. Mallada, Global analysis of synchronization performance for power systems: Bridging the theory-practice gap, IEEE Trans. on Automatic Control, 2020.

11. A. Bahram, M. H. Hajiesmaili, Z. Lee, N. Crespi, and E. Mallada, Online EV Scheduling Algorithms for Adaptive Charging Networks with Global Peak Constraints, IEEE Transactions on Sustainable Computing, 2020.

12. E. Weitenberg, Y. Jiang, C. Zhao, E. Mallada, C. De Persis, and F. Dorfler Robust decentralized secondary frequency control in power systems: Merits and trade-offs IEEE Transactions on Automatic Control, 2019.

13. R. Pates and E. Mallada, Robust scale free synthesis for frequency regulation in power systems, IEEE Trans, on Control of Network Systems, 2018.

14. N. Nazir and M. Almassalkhi, Receding-horizon optimization of unbalanced distribution systems with time-scale separation for discrete and continuous control devices, Power System Computation Conference, Dublin, Ireland June, 2018.

15. S. Brahma, M. Almassalkhi, H. Ossareh, A Stochastic Linearization Approach to Optimal Primary Control of Power Systems with Generator Saturation, IEEE Conference on Control Technology and Applications, Copenhagen, Denmark August, 2018.

16. I. Chakraborty, S. Nandanoori, and S. Kundu, Virtual Battery Parameter Identification using Transfer Learning based Stacked Autoencoder, IEEE International Conference on Machine Learning and Applications, Orlando, FL December, 2018. (Nominated for best paper award).

17. S. Nandanoori, I. Chakraborty, T. Ramachandran, and S. Kundu Identification and Validation of Virtual Battery Model for Heterogeneous Devices, IEEE PES General Meeting 2019, Atlanta, GA, August, 2018.

18. T. Ramachandran, A. Reiman, M. Rice and S. Kundu, Distribution System State Estimation in the presence of high PV penetration, American Control Conference, Philadelphia, PA, 2019.

19. W. Huang, S. Brahma, and H. Ossareh, Quasilinear control of systems with time-delays and nonlinear actuators and sensors, American Control Conference Philadelphia, PA, 2019.

20. C. Ji, M. H., D. F. Gayme and E. Mallada, Coordinating Distribution System Resources for Co-optimized Participation in Energy and Ancillary Service Transmission System Markets, American Control Conference, Philadelphia, PA, 2019.

21. C. Avraam, J. Rines, A. Sarker, F. Paganini, and E. Mallada, Voltage Collapse Stabilization in Star DC Networks, American Control Conference Philadelhia, PA, 2019.

22. S. Brahma and H. Ossareh, Quasilinear control of feedback systems with multivariate nonlinearities, IEEE Conference on Decision and Control, Nice, France, 2019.

23. P. You, D. F. Gayme, and E. Mallada, The Role of Strategic Load Participants in Two-Stage Settlement Electricity Markets, IEEE Conference on Decision and Control, Nice, France, 2019.

24. H. Min and E. Mallada, Dynamics Concentration of Large-Scale Tightly-Connected Networks, IEEE Conference on Decision and Control, Nice, France, 2019.

25. N. Nazir and M. Almassalkhi, Convex inner approximation of the feeder hosting capacity limits on dispatchable demand IEEE Conference on Decision and Control Nice, France, 2020.

26. N. Nazir and M. Almassalkhi, Stochastic multi-period optimal dispatch of energy storage in unbalanced distribution feeders, Power Systems Computation Conference, Porto, Portugal, 2020.

27. C. Shapiro, C. Ji, and D. F. Gayme, Real-time Energy Market Arbitrage via Aerodynamic Energy Storage in Wind Farms, American Control Conference, 2020.

28. J. Guthrie and E. Mallada, Minimum-Time Charging of Energy Storage in Microgrids via Approximate Conic Relaxation, IEEE European Control Conference, 2020.

29. Y. Shen, M. Bichuch, and E. Mallada, On the Value of Energy Storage in Generation Cost Reduction, IEEE European Control Conference, 2020.

30. C. Shapiro, C. Ji, and D. F. Gayme, Real-time Energy Market Arbitrage via Aerodynamic Energy Storage in Wind Farms, American Control Conference, Denver, CO, 2020.

Other Results

1. The Future of Energy Workshop at UVM, 9/27-28/2018.
2. NIST Workshop on Smart Grid Test-beds & Collaborations at UVM, 4/23/2019.
3. Dr. Dennice Gayme was featured in IEEE Control System Society's Control Magazine.

Path Forward

The R&D outcomes of this project directly supports a so-called "Market DSO" approach to DER coordination, where the DSO is the sole scheduling coordinator of DERs and aggregates resources to form a simple interface with the TSO. This importantly informs the TSO of expected aggregate distribution system DER actions across the system and also helps the DSO meet changing grid and market conditions. However, such a DSO-centric approach indirectly precludes participation from individual DER owners and aggregators. To overcome this, there exists opportunities going forward to extend the R&D outcomes from this project to consider multiple generalized DER aggregators acting within the limits of the network. Below we list some key directions and avenues for valuable future contributions:

- **Software tools for DSO:** The FOL layer represents a sophisticated combination of grid analytics (e.g., network reduction, scenario generation) and state-of-the-art resource optimization algorithms suitable for realistic distribution feeders. Specifically, these tools can be extended to serve DSOs in the form of interactive power grid analytics (iPGA) platform (see Fig. 27)), which is capable of visualizing and re-playing historical grid conditions from data. Combined with optimization and/or network reduction, the tools can perform what-if scenarios around hosting capacity for DERs and solar PV. In this direction, **the team has disclosed the software tools as inventions, licensed them to clean tech startup company Packetized Energy, who is advancing the concepts with their commercial product GridSolver that is currently in use by utilities in the U.S.** to improve visualization and decision support for utility engineers. In addition, the team had been asked by Industry partner ORU to use these tools to conduct engineering analysis around solar PV penetrations, capacitor banks, and protection system. Thus, software tools represent a promising avenue going forward for the FOL methods.

- **Online, realtime disaggregation of resources:** The team is leading a panel at INFORMS 2020 Annual meeting on this topic. For large (i.e., realistic) networks and fast market signals (e.g., frequency regulation), receding-horizon implementations of OPF (i.e., FOL) has certain limitations as multi-period optimization problems take time to solve at scale. Since the FOL effectively performs disaggregation of the aggregate head-node signal across the network's resources, **the team has extended the FOL to online computation for simple radial and balanced networks, which permits real-time disaggregation that supports frequency regulation.** The ideas leverage team discussions from Year 1 in the project to enable the DSO to compute "dynamic hosting capacity" limits at each node of its network and within which any flexible DERs and PV inverters can be employed with a-priori guaranteed satisfaction of network constraints.

This future avenue of work will enable real-time, online, grid-aware control of VBs to allow DER owners and aggregators to subscribe to portions of these nodal DER hosting capacities from the DSO and freely dispatch DERs within their subscribed limits towards any market service (i.e., arbitrary timescales). As we move to real-time control of VBs their power dynamics become relevant and control theory need to advance to account for the complexities of VB dynamics, non-linearities, and timescales. The intra-feeder work is a clear avenue to advance the control theory and application to solar PV inverters.

- **Improve fundamental understanding of the limits of network aggregations:** AC networks complicate aggregated representations of nodal flexibility. The STL performs advanced DER services related to characterizing groups of DERs as VBs and then controlling DERs to satisfy certain power set-points. The characterization of the energy/power flexibility from heterogeneous groups of DERs **will require future advances in data-driven and learning-based methodologies and represents a salient direction for R&D** - and is being pursued by both UVM and PNNL teams. In particular, the topic of aggregation of flexibility over a network will be critical to pursue. This is related to the dynamic hosting capacity mentioned above and an area we are interested to pursue.

- **Optimal risk-aware multi-market participation:** as DERs are aggregated for market participation and enable reliable solar PV integration, it will become important to maximize revenue potential of flexible demand. However, flexible demand is an inherently stochastic resource (given uncertain parameters and end-usage patterns), so both Aggregators and TSOs want to manage risks associated with not meeting obligations. For that, we see **extensions of the GML towards risk-based dispatches and have started this work in the project already with the stochastic formulation of the GML**, which considers both uncertainty in resources and market signals. In addition, we need to account for multiple concurrent market opportunities and understand which forms of flexible demand are most valuable for each type of market service, so that fleets composition can be optimized and to inform regulators.

- **Computing at scale with network reduction:** At the core of machine learning, optimization, AC load flows are nodes, edges, and lots of networks. Thus, the network reduction techniques developed and tested in this project for OPF purposes could be generalized and studied further to other networks and other applications. Specifically, the ability to take large network and reduce them with negligible model error gives rise to scalable computing for both machine learning and optimization. In the FOL, we developed and applied optimization to reduced networks and and lifted the optimal dispatch solutions back up to the full network where the resources were actuated. While we have not provided guarantees on performance (optimality) or quantified model mismatch (feasibility), we showed that **network reduction offers a valuable paths for scalable computing/optimization and are interested in pursuing network reduction techniques on general network problems** and develop methodologies that characterize loss of optimality and feasibility from computing on reduced networks and the inefficiencies associated with lifting optimal solutions up to their full networks.

References

[1] *Distributed energy resources: Connection, Modeling and Reliability Considerations.* Tech. rep. North American Electric Reliability Council (NERC), Nov. 2016.

[2] Nawaf Nazir and Mads Almassalkhi. *Grid-aware aggregation and realtime disaggregation of distributed energy resources in radial networks.* 2019. arXiv: `1907.06709 [math.OC]`.

[3] Lazard. *Levelized Cost of Energy Analysis - Version 13.0.* Tech. rep. Lazard, 2019. URL: `{https://www.lazard.com/media/451086/lazards-levelized-cost-of-energy-version-130-vf.pdf}`.

[4] United Nations Environment Programme. *Emissions Gap Report.* UNEP, Nairobi, 2019. URL: `https://www.unenvironment.org/resources/emissions-gap-report-2019`.

[5] Cara Goldenberg, Mark Dyson, and Harry Masters. *Demand Flexibility: The Key To Enabling A Low-cost, Low-carbon Grid.* Tech. rep. Rocky Mountain Institute, 2018. URL: `https://rmi.org/wp-content/uploads/2018/02/Insight_Brief_Demand_Flexibility_2018.pdf`.

[6] Ryan Hledik, Ahmad Faruqui, Tony Lee, and John Higham. *The National Potential for Load Flexibility: VALUE AND MARKET POTENTIAL THROUGH 2030.* Tech. rep. Boston, Massachussetts: The Brattle Group, June 2019.

[7] IEA. *Digitalisation and Energy.* Tech. rep. 2017. URL: `https://www.iea.org/reports/digitalisation-and-energy`.

[8] Paul DeMartini. *Future of U.S. Electric Distribution: Part II.* Tech. rep. Edison Electric Institute, 2012. URL: `{https://gridarchitecture.pnnl.gov/media/white-papers/2012%20Jul-Future%20of%20Electric%20Distribution.pdf}`.

[9] Felix F. Wu, Pravin P. Varaiya, and Ron S.Y. Hui. "Smart Grids with Intelligent Periphery: An Architecture for the Energy Internet". In: *Engineering* 1.4 (2015), pp. 436 – 446. URL: `http://www.sciencedirect.com/science/article/pii/S2095809916300248`.

[10] Jeffrey D Taft. *Architectural basis for highly distributed transactive power grids: Frameworks, networks, and grid codes.* Tech. rep. Pacific Northwest National Lab.(PNNL), Richland, WA (United States), 2016.

[11] Jeffrey D Taft. *Grid architecture 2.* Tech. rep. Pacific Northwest National Lab.(PNNL), Richland, WA (United States), 2016.

[12]   Paul De Martini. "Operational coordination architecture: New models and approaches". In: *IEEE Power and Energy Magazine* 17.5 (2019), pp. 29–39.

[13]   Paul De Martini, Lorenzo Kristov, and Lisa Schwartz. *DISTRIBUTION SYSTEMS IN A HIGH DISTRIBUTED ENERGY RESOURCES FUTURE: Planning, Market Design, Operation and Oversight.* Tech. rep. Lawrence Berkeley National Laboratory, Oct. 2015.

[14]   Lorenzo Kristov, Paul De Martini, and Jeffrey D Taft. "A tale of two visions: Designing a decentralized transactive electric system". In: *IEEE Power and Energy Magazine* 14.3 (2016), pp. 63–69.

[15]   conEdison. "Consolidated Edison Distributed System Implementation Plan". In: *Con Edison DSIP filing.* 2018, pp. 1–7.

[16]   K. Kok and S. Widergren. "A Society of Devices: Integrating Intelligent Distributed Resources with Transactive Energy". In: *IEEE Power and Energy Magazine* 14.3 (May 2016), pp. 34–45. DOI: 10.1109/MPE.2016.2524962.

[17]   Md Salman Nazir and Ian A Hiskens. "A dynamical systems approach to modeling and analysis of transactive energy coordination". In: *IEEE Transactions on Power Systems* (2018).

[18]   Lingwen Gan and Steven H Low. "Convex relaxations and linear approximation for optimal power flow in multiphase radial networks". In: *Power Systems Computation Conference (PSCC)* (2014), pp. 1–9.

[19]   Steven H Low. "Convex relaxation of optimal power flow—Part I: Formulations and equivalence". In: *IEEE Transactions on Control of Network Systems* 1.1 (2014), pp. 15–27.

[20]   Steven H Low. "Convex relaxation of optimal power flow—Part II: Exactness". In: *IEEE Transactions on Control of Network Systems* 1.2 (2014), pp. 177–189.

[21]   Saverio Bolognani and Sandro Zampieri. "On the existence and linear approximation of the power flow solution in power distribution networks". In: *IEEE Transactions on Power Systems* 31.1 (2016), pp. 163–172.

[22]   Michael D Sankur, Roel Dobbe, Emma Stewart, Duncan S Callaway, and Daniel B Arnold. "A Linearized Power Flow Model for Optimization in Unbalanced Distribution Systems". In: *arXiv preprint arXiv:1606.04492* (2016).

[23]   Emiliano Dall'Anese, Swaroop S Guggilam, Andrea Simonetto, Yu Christine Chen, and Sairaj V Dhople. "Optimal regulation of virtual power plants". In: *IEEE Transactions on Power Systems* 33.2 (2018), pp. 1868–1881.

[24]   Daniel B Arnold, Michael D Sankur, Matias Negrete-Pincetic, and Duncan S Callaway. "Model-Free Optimal Coordination of Distributed Energy Resources for Provisioning Transmission-Level Services". In: *IEEE Transactions on Power Systems* 33.1 (2018), pp. 817–828.

[25]   Ali Bidram and Ali Davoudi. "Hierarchical structure of microgrids control system". In: *IEEE Transactions on Smart Grid* 3.4 (2012), pp. 1963–1976.

[26]   K. Baker, A. Bernstein, E. Dall'Anese, and C. Zhao. "Network-Cognizant Voltage Droop Control for Distribution Grids". In: *IEEE Transactions on Power Systems* 33.2 (2018), pp. 2098–2108.

[27]   F. Dörfler, J. W. Simpson-Porco, and F. Bullo. "Breaking the Hierarchy: Distributed Control and Economic Optimality in Microgrids". In: *IEEE Transactions on Control of Network Systems* 3.3 (2016), pp. 241–253.

[28]   He Hao, Borhan M Sanandaji, Kameshwar Poolla, and Tyrone L Vincent. "Aggregate flexibility of thermostatically controlled loads". In: *IEEE Transactions on Power Systems* 30.1 (2014), pp. 189–198.

[29]   J. T. Hughes, A. D. Domínguez-García, and K. Poolla. "Identification of Virtual Battery Models for Flexible Loads". In: *IEEE Transactions on Power Systems* 31.6 (Nov. 2016), pp. 4660–4669. DOI: 10.1109/TPWRS.2015.2505645.

[30]   Indrasis Chakraborty, Sai Pushpak Nandanoori, and Soumya Kundu. "Virtual battery parameter identification using transfer learning based stacked autoencoder". In: *2018 17th IEEE International Conference on Machine Learning and Applications (ICMLA)*. IEEE. 2018, pp. 1269–1274.

[31]   Sai Pushpak Nandanoori, Indrasis Chakraborty, Thiagarajan Ramachandran, and Soumya Kundu. "Identification and validation of virtual battery model for heterogeneous devices". In: *2019 IEEE Power & Energy Society General Meeting (PESGM)*. IEEE. 2019, pp. 1–5.

[32]   I. Chakraborty, S. P. Nandanoori, S. Kundu, and K. Kalsi. "Stochastic Virtual Battery Modeling of Uncertain Electrical Loads Using Variational Autoencoder*". In: *2020 American Control Conference (ACC)*. 2020, pp. 1305–1310.

[33]   N. Nazir, P. Racherla, and M. Almassalkhi. "Optimal multi-period dispatch of distributed energy resources in unbalanced distribution feeders". In: *IEEE Transactions on Power Systems* (2020), pp. 1–1.

[34]   Nawaf Nazir and Mads Almassalkhi. "Receding-Horizon Optimization of Unbalanced Distribution Systems with Time-Scale Separation for Discrete and Continuous Control Devices". In: *2018 Power Systems Computation Conference (PSCC)*. IEEE. 2018, pp. 1–7.

[35]   Nawaf Nazir and Mads Almassalkhi. "Stochastic multi-period optimal dispatch of energy storage in unbalanced distribution feeders". In: *2020 Power Systems Computation Conference (PSCC)*. 2020, pp. 1–7.

[36]   Mads Almassalkhi et al. "Hierarchical, Grid-Aware, and Economically Optimal Coordination of Distributed Energy Resources in Realistic Distribution Systems". In: *Energies* ((Accepted) 2020).

[37] S. S. Sami, M. Cheng, J. Wu, and N. Jenkins. "A virtual energy storage system for voltage control of distribution networks". In: *CSEE Journal of Power and Energy Systems* 4.2 (June 2018), pp. 146–154. ISSN: 2096-0042. DOI: 10.17775/CSEEJPES.2016.01330.

[38] Biju Naduvathuparambil, Matthew C Valenti, and Ali Feliachi. "Communication delays in wide area measurement systems". In: *Proceedings of the Thirty-Fourth Southeastern Symposium on System Theory (Cat. No. 02EX540)*. IEEE. 2002, pp. 118–122.

[39] Mahraz Amini and Mads Almassalkhi. "Investigating delays in frequency-dependent load control". In: *2016 IEEE Innovative Smart Grid Technologies-Asia (ISGT-Asia)*. IEEE. 2016, pp. 448–453.

[40] Sai Pushpak Nandanoori, Soumya Kundu, Draguna Vrabie, Karan Kalsi, and Jianming Lian. "Prioritized threshold allocation for distributed frequency response". In: *2018 IEEE Conference on Control Technology and Applications (CCTA)*. IEEE. 2018, pp. 237–244.

[41] C Gokcek, P T Kabamba, and S M Meerkov. "An LQR/LQG Theory for Systems With Saturating Actuators". In: *IEEE Transactions on Automatic Control* 46.10 (2001).

[42] Roger Fletcher. *Practical methods of optimization.* John Wiley & Sons, 2013.

[43] Pauli Virtanen et al. "SciPy 1.0: Fundamental Algorithms for Scientific Computing in Python". In: *Nature Methods* 17 (2020), pp. 261–272. DOI: 10.1038/s41592-019-0686-2.

[44] David J Wales and Jonathan PK Doye. "Global optimization by basin-hopping and the lowest energy structures of Lennard-Jones clusters containing up to 110 atoms". In: *The Journal of Physical Chemistry A* 101.28 (1997), pp. 5111–5116.

[45] William H Kersting. "Radial distribution test feeders". In: *Power Engineering Society Winter Meeting* 2 (2001), pp. 908–912.

[46] M. Amini and M. Almassalkhi. "Optimal Corrective Dispatch of Uncertain Virtual Energy Storage Systems". In: *IEEE Transactions on Smart Grid* 11.5 (2020), pp. 4155–4166.

[47] K. Christakou, J. LeBoudec, M. Paolone, and D. Tomozei. "Efficient Computation of Sensitivity Coefficients of Node Voltages and Line Currents in Unbalanced Radial Electrical Distribution Networks". In: *IEEE Transactions on Smart Grid* 4.2 (June 2013), pp. 741–750. ISSN: 1949-3053. DOI: 10.1109/TSG.2012.2221751.

[48] C. Ji, M. Hajiesmaili, D. F. Gayme, and E. Mallada. "Coordinating Distribution System Resources for Co-optimized Participation in Energy and Ancillary Service Transmission System Markets". In: *2019 American Control Conference (ACC)*. 2019, pp. 1315–1322. DOI: 10.23919/ACC.2019.8815242.

[49] New York ISO. *Real-Time Market LBMP - Zonal.* http://mis.nyiso.com/public/P-24Alist.htm. accessed 2020.

[50]   Carleton Coffrin, Russell Bent, Kaarthik Sundar, Yeesian Ng, and Miles Lubin. "PowerModels.jl: An Open-Source Framework for Exploring Power Flow Formulations". In: *2018 Power Systems Computation Conference (PSCC)*. June 2018, pp. 1–8.

[51]   C. Brunner. "IEC 61850 for power system communication". In: *2008 IEEE/PES Transmission and Distribution Conference and Exposition*. 2008, pp. 1–6.

[52]   R. E. Mackiewicz. "Overview of IEC 61850 and benefits". In: *2006 IEEE Power Engineering Society General Meeting*. 2006, pp. 1–8.